# Combustion of Solid Propellants

**G. Lengellé, J. Duterque, J.F. Trubert**
Research Scientists, Energetics Department
Office national d'études et de recherches aérospatiales (ONERA)
29 avenue de la Division Leclerc
BP 72 – 92322 Châtillon Cedex
FRANCE

## *ABSTRACT*

*A review of **the understanding of the combustion mechanisms** of solid propellants that the authors have built from their work and from the literature is presented. Such an understanding is an important part of the process carried out to master the behavior of solid propellants and to obtain desired characteristics (with respect to energetic level, burning rate level, sensitivity to pressure and initial temperature, nature of emitted combustion products, vulnerability to various aggressions...).*

***The propellants and propellant components considered** are:*

- *double-base propellants, based on nitrocellulose and nitroglycerin,*
- *active binder, based on an inert polymer (or energetic such as PAG) and a liquid nitrate ester,*
- *inert binders, such as polybutadiene,*
- *ammonium perchlorate,*
- *nitramines, such as HMX, RDX and CL20 (HNIW),*
- *composite ammonium perchlorate-inert binder propellants,*
- *composite propellants based on a nitramine and an active binder,*
- *aluminum, with respect to the two previous types of propellants,*
- *additives, when appropriate.*

***The features of the combustion zone described** are:*

- *In the condensed phase, the thickness of the temperature profile and of the decomposition zone, the kinetics of the decomposition, the energy released, the nature of the gases evolved, the surface temperature;*
- *In the gas phase, the type of flame structure (diffusion or kinetically controlled), the possibility of staging (such as in double-base propellants), the kinetics of the reaction(s), the energy released, the flame temperature (primary and final, when applicable).*

*It is concluded that a fairly proper knowledge of the combustion of the various components and propellants has been acquired (being now extended to new ingredients, oxidizers or binders). Furthermore, based on this knowledge, a first approach modeling description can be achieved. Such a description is necessary in accompanying the elaboration of new propellants and in preparing the investigation of more complicated regimes such as those of erosive burning and of non-stationary response.*

*Paper presented at the RTO/VKI Special Course on "Internal Aerodynamics in Solid Rocket Propulsion", held in Rhode-Saint-Genèse, Belgium, 27-31 May 2002, and published in RTO-EN-023.*

# Report Documentation Page

*Form Approved*
*OMB No. 0704-0188*



| 1. REPORT DATE | 2. REPORT TYPE | 3. DATES COVERED |
|---|---|---|
| **00 JAN 2004** | **N/A** | **-** |

| 4. TITLE AND SUBTITLE | 5a. CONTRACT NUMBER |
|---|---|
| **Combustion of Solid Propellants** | 5b. GRANT NUMBER |
| | 5c. PROGRAM ELEMENT NUMBER |
| 6. AUTHOR(S) | 5d. PROJECT NUMBER |
| | 5e. TASK NUMBER |
| | 5f. WORK UNIT NUMBER |
| 7. PERFORMING ORGANIZATION NAME(S) AND ADDRESS(ES) **Research Scientists, Energetics Department Office national détudes et de recherches aérospatiales (ONERA) 29 avenue de la Division Leclerc BP 72 92322 Châtillon Cedex FRANCE** | 8. PERFORMING ORGANIZATION REPORT NUMBER |
| 9. SPONSORING/MONITORING AGENCY NAME(S) AND ADDRESS(ES) | 10. SPONSOR/MONITOR'S ACRONYM(S) |
| | 11. SPONSOR/MONITOR'S REPORT NUMBER(S) |

12. DISTRIBUTION/AVAILABILITY STATEMENT
**Approved for public release, distribution unlimited**

13. SUPPLEMENTARY NOTES
**See also ADM001656., The original document contains color images.**

14. ABSTRACT

15. SUBJECT TERMS

| 16. SECURITY CLASSIFICATION OF: | | | 17. LIMITATION OF ABSTRACT | 18. NUMBER OF PAGES | 19a. NAME OF RESPONSIBLE PERSON |
|---|---|---|---|---|---|
| a. REPORT | b. ABSTRACT | c. THIS PAGE | | | |
| **unclassified** | **unclassified** | **unclassified** | **UU** | **62** | |

**Standard Form 298 (Rev. 8-98)**
Prescribed by ANSI Std Z39-18

# INTRODUCTION

Much work has been devoted in various countries to investigating the combustion mechanisms of solid propellants. It is timely to bring together the information obtained by the authors and compared to that of the literature on the combustion of the individual components as well as of their combination into propellants. This review is about the existing components and propellants: double-base propellants and active binders, inert binders, ammonium perchlorate, HMX, RDX and CL20 and the corresponding composite propellants, ammonium perchlorate – inert binder (plus possibly aluminum), HMX (or RDX or CL20) – active binder.

The viewpoint adopted here is that of the understanding of the combustion behavior of propellants. Therefore as much information as possible is presented about the fundamentals of the processes (thermal properties, kinetics in the condensed phase and in the gas phase...), whereas no attempt is made to establish a complete catalog of practical results on various propellants with different particle sizes, catalysts, variations on the percentage of ingredients. The aim is to give a clear, as conclusive as possible picture. This will then be non compatible with a complete discussion of the various, sometimes contradictory, mechanisms proposed in the literature. Also precluding such a discussion is the will to compare the different components and the corresponding propellants.

Some space is taken up by physico-chemical modeling. The aim is not so much to give the elements of mathematical descriptions which could be used for a priori computations of burning characteristics of propellants (to the extent that such computations are possible). The point is more to put to test the hypotheses made on the mechanisms of combustion by incorporating them in reasonable models and confronting the results thus obtained to experimental data.

These descriptions can also be viewed, along-side with the data given for each component or propellant, as useful for mastering the regimes of combustion which go beyond stationary combustion: that is erosive burning and unsteady (under pressure excursions or pressure oscillations) combustion responses.

Table 1 gives information about the various types of propellants of actual use.

**Table 1: Performances/Characteristics of Various Propellants**

| PROPELLANT | COMPOSITION (main ingredients) | $\rho_p$ g/cm$^3$ | $I_s$(70/1) theoretical. (losses) | APPLICATIONS /CHARACTERISTICS |
|---|---|---|---|---|
| Extruded DB | Nitrocellulose Nitroglycerin | ≤ 1.66 | ≤ 230 s (≈ - 10 s) | - Anti-tank rockets and missiles<br>- AS rockets<br>- Some tactical missiles (SA)<br>Minimum smoke |
| Powder cast DB | Nitrocellulose Nitroglycerin | ≤ 1.66 | ≤ 225 s (≈ - 10 s) | - Anti-tank missiles<br>- Some tactical missiles (AS)<br>Minimum smoke |
| AP composite | Ex: 88 % AP - 12 % HTPB | 1.72 | ≈250 s (≈ - 10s) | - Some AS rockets<br>- Some tactical missiles<br>Reduced smoke (HCl-$H_2O$) |
| AP composite with aluminum | Ex: 68 AP - 20 al. - 12 HTPB | ≈1.82 | 265 s (≈ - 20 s) | - AA tactical missiles<br>- Anti-ship missiles (booster)<br>- Tactical ballistic missiles<br>- Strategic ballistic missiles<br>- Apogee motors<br>- Boosters for space launchers (Titan III, IV, V, Space Shuttle, Ariane V, H2A...)<br>Smoky ($Al_2O_3$) |
| HMX (RDX) composite | HMX or RDX - XLDB binder | < 1.75 | < 255 s (≈ - 15 s) | - Anti-ship missiles (cruise)<br>- SA missiles<br>Minimum smoke (without AP) |
| HMX composite with aluminum | HMX + AP+ Al XLDB binder | 1.87 | 273 s | - Strategic ballistic missiles (upper stages) (Trident, MX...)<br>Smoky ($Al_2O_3$) |

Sources: Air et Cosmos n° 1000, May 1984.
Annales des Mines, Jan-Feb. 1986.
Aéronautique et Astronautique, n° 138, 1989.

*Double-base propellants* (made by the extrusion or powder casting techniques) are used in anti-tank rockets or missiles and in some tactical missiles. Their main advantage is that they produce a minimum amount of smoke (only from a small amount of additives).

*Composite propellants, based on ammonium perchlorate (AP)* without aluminum, generate reduced smoke, HCl and $H_2O$ vapor will precipitate into droplets in the plume under given temperature and humidity conditions. They are used for various tactical missiles. With aluminum, they are widely used in missiles and space launchers. They produce alumina smoke, which, in the case of space launchers, could be considered in the future to be undesirable (along with HCl).

*Composite propellants based on nitramines and an "active" binder* (cross linked polymer with nitroglycerin or other liquid nitrate esters) are used more and more. Without aluminum, they are in the minimum smoke category and they replace DB propellants. With aluminum, they reach the highest specific impulse and density and are used so far for upper stages of strategic missiles.

The combustion of the components and then of the various propellants will be seen in the next chapters.

A few general references about chemical propulsion, solid propellants and combustion can be found at the end of the main text, ahead of more specialized references introduced progressively in the following chapters.

# COMBUSTION OF DOUBLE-BASE PROPELLANTS AND ACTIVE BINDERS

## 1.0 Introduction

It seems appropriate to consider double-base propellant combustion mechanisms in the first place because they correspond to relatively simpler premixed processes which lend themselves to a better understanding and because they have been investigated for a long time (starting in the 1950's) in the US, the then USSR, the UK, Japan and France in particular. General background on the combustion of double-base propellants can be found in references [1-6].

As will be seen, the mechanisms involved in the combustion of double-base propellants will apply as well to the active binders ( ≈1/3 polymer, ≈ 2/3 nitroglycerin, or other liquid nitrate esters).

Double-base propellants are made in a number of ways. When they are rolled or extruded, the components are nitrocellulose and nitroglycerin, to which some stabilizers such as centralite and plasticizers are added. When they are cast, a casting powder (made of nitrocellulose, some nitroglycerin, and the various additives) is swelled within the mold by a liquid mixture of nitroglycerin and triacetin. The grain thus obtained is then inhibited and used free standing in the motor. The propellant ingredients can also be mixed, cast, cross-linked, and the grain case bonded.

Depending on the relative amounts of nitrocellulose and nitroglycerin, Figure 1, the energetic level of the propellant can be increased or, in the usual terminology, its "heat of explosion" or "calorimetric value", that is, the heat evolved in a calorimetric bomb by combustion under an inert atmosphere. One can then talk about "cool" and "hot" compositions.

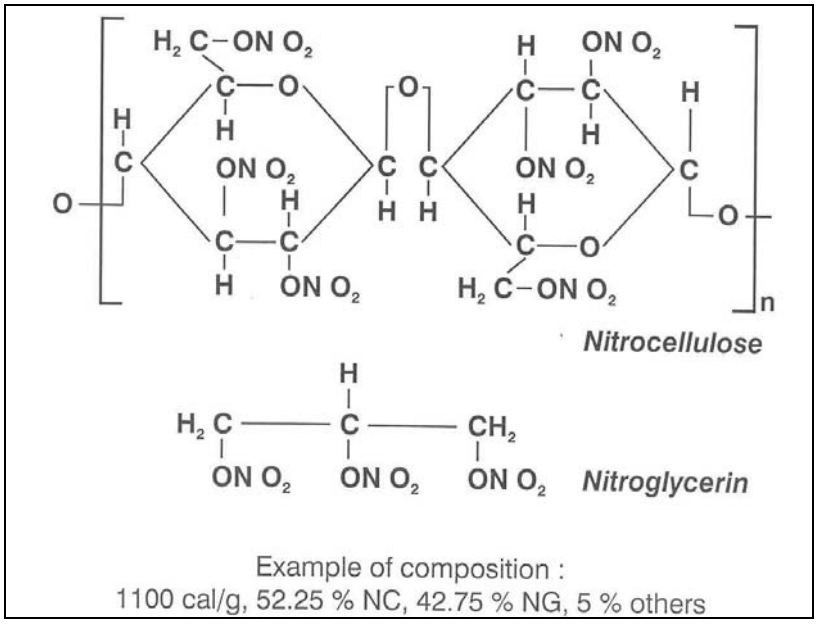


**Figure 1: Components of Double Base Propellants.**

Double-base propellants are used in small and medium sized rockets and thus exposed to varying ambient temperatures. The sensitivity of the motor operation to temperature depends upon the propellant burning rate sensitivity to both the temperature and the pressure. As can be seen on Fig. 2, the pressure exponent, in the usual empirical law $v_b \sim p^n$, is around 0.7 and increases to nearly 1 at high pressure. Super-rate effects (Fig. 3) are created by the use of additives, most often lead and copper salts combined with carbon black. At the end of the super-rate zone, the burning rate falls back to that of the control propellant, with the occurrence of a nearly zero pressure exponent zone, a "plateau" effect, or a negative exponent zone, a "mesa" effect. These terms are used by analogy with topographical features. A fairly complete set of results can be found in reference [6]. It is only in these reduced pressure exponent zones that the propellant is used to minimize the motor operation sensitivity to ambient temperature. Due to this fact, the study of the combustion of propellants without additives should be conceived only as a first step leading to an understanding of modified (that is, with additives) propellants.

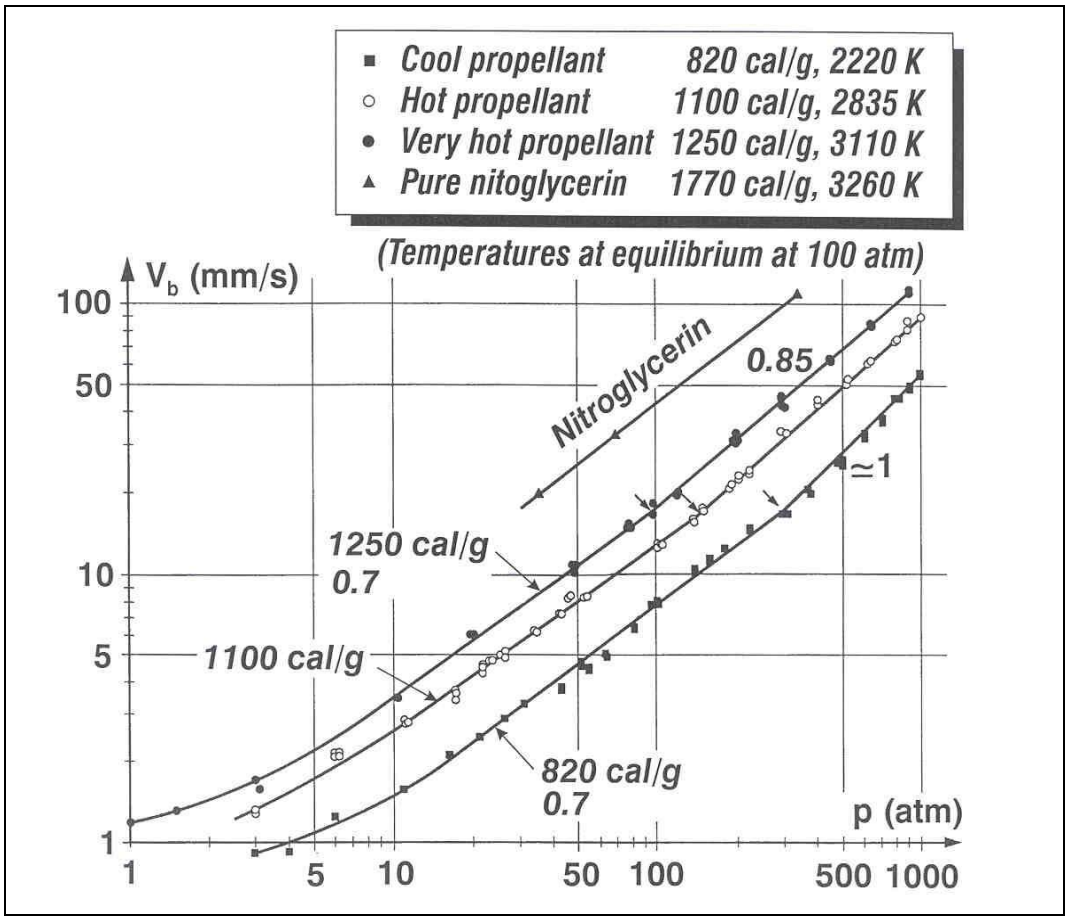


**Figure 2: Burning Rate vs Pressure.**
**(Double Base Propellants)**

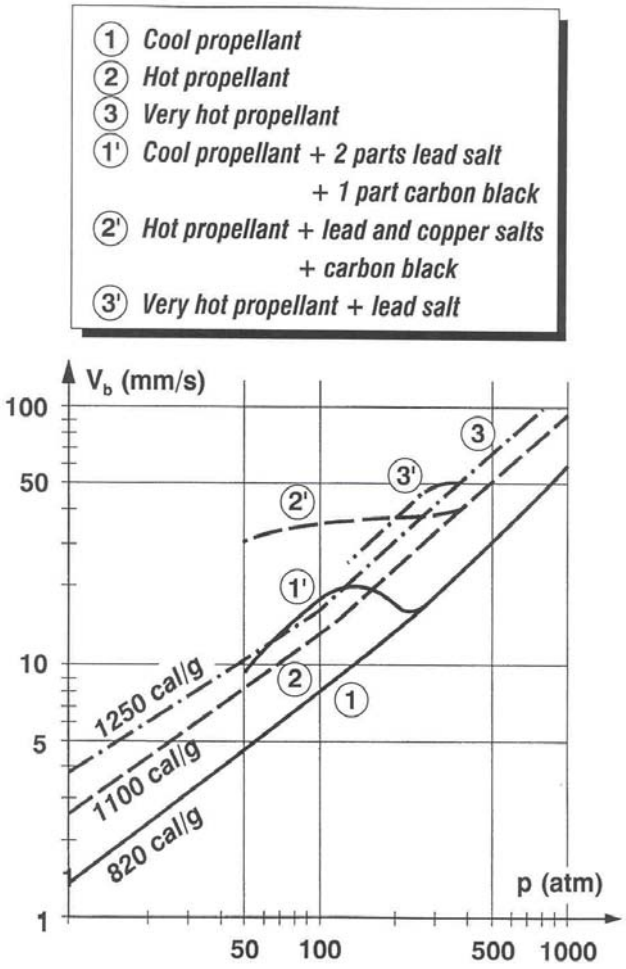


**Figure 3: Super-Rate Effects.**
**(Double Base Propellants)**

## 2.0 Flame Structure

From the works mentioned previously it is possible to describe the combustion wave structure of double-base propellants, in particular its chemical processes, see Figs. 4 and 5. The various data will be discussed and justified later. Gas analysis results are from reference [7]; they refer to mass fractions.

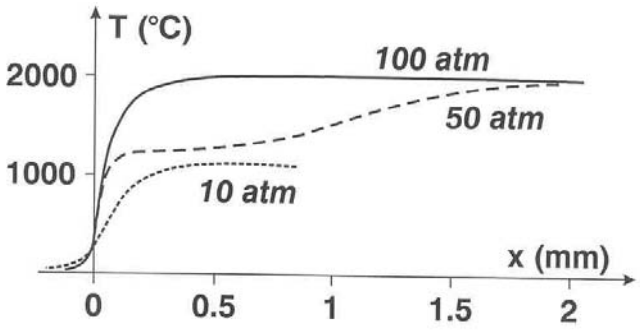


**Figure 4: Temperature Profiles.**
**(Double Base Propellant)**

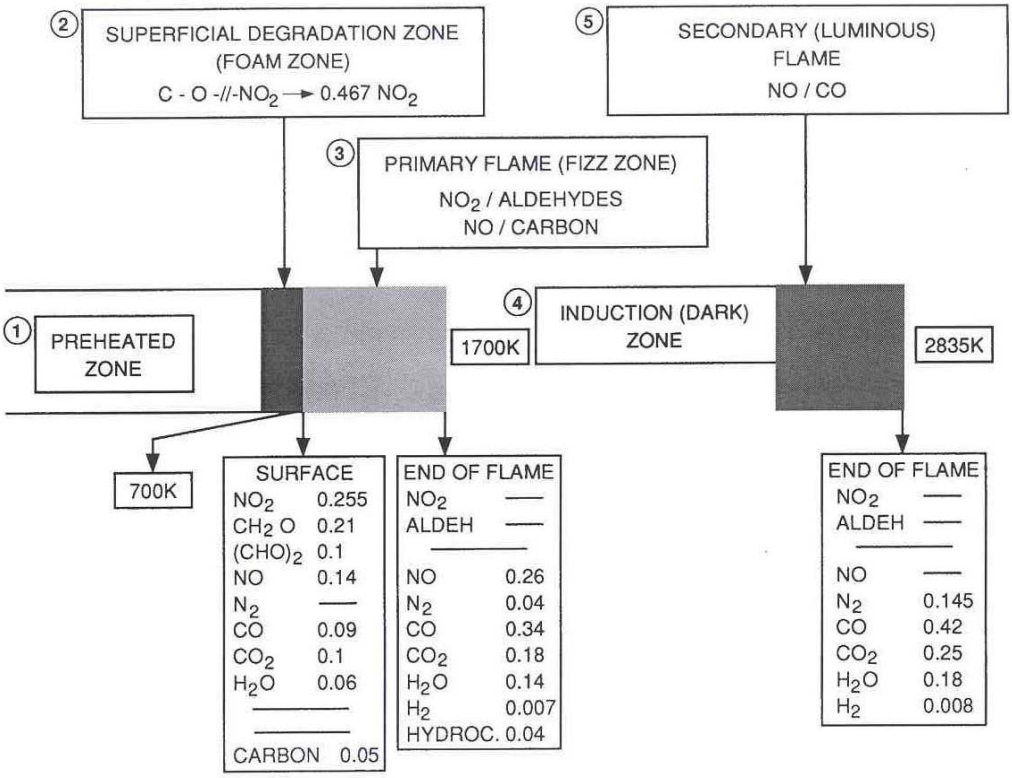


**Figure 5: Various Zones of the Combustion of a Double Base Propellant.**

The propellant components pass unaffected through a preheated zone of a few tens of micrometers in a few milliseconds and reach a superficial degradation zone (or "foam" zone in the early literature) where the temperature becomes high enough for the molecular degradation to take place, initiated by the rupture of the C-O-//-$NO_2$ bond. Simultaneous recombination occurs so that a mixture of $NO_2$, aldehydes, but also NO emerges from the surface and so that the net energy balance of the degradation is exothermic. At pressures under about 100 atm, a clearly separated primary flame ("fizz" zone) and a secondary flame ("luminous" flame) are observed, the first involving $NO_2$-aldehydes reactions and the second probably NO-CO reactions. In this pressure range the secondary flame is too far away to have any effect on the surface or even to induce a temperature gradient into the primary flame. The burning rate is then entirely under the influence of the latter. This corresponds to a burning rate/pressure law with a 0.7 pressure exponent (Fig. 1). As the pressure increases, the secondary flame enhances and then merges into the primary flame and a transition is observed to a zone with a pressure exponent close to 1. When the secondary flame is fully developed, even at pressures for which it does not yet influence the burning rate, the final products ($N_2$, CO, $CO_2$, $H_2O$ and $H_2$) and the final temperature (2100-3100 K, depending on the heat of explosion) are attained.

Table 2 gives data relative to the various zones of the combustion wave.

**Table 2: Characteristics of the Combustion Zones (Measured Results from Zenin)**

| | | | |
|---|---|---|---|
| Pressure atm. | 10 | 50 | 100 |
| $v_b$ mm/s | 1.9 | 6.7 | 10.6 |
| $T_s$, K | 610 | 662 | 685 |
| Preheated zone, µm (measured/computed) | 140/194 | 50/55 | 45/35 |
| Residence time in preheated zone, ms | 100 | 8 | 3 |
| Superficial degradation zone µm | 11 | 3 | 2 |
| Residence time in superficial zone, ms | 6 | 0,5 | 0,2 |
| Flame thickness, µm (measured) | 200 | 75 | 110 (secondary flame) |

Double base propellant staged flame (1st flame, dark zone, 2nd flame), under pressures: 0.7 1.2 1.6 2.1 2.6 MPa.

HMX, under 0.15 MPa

**Visualizations with high speed camera, for a double base propellant, showing the secondary flame moving closer to the surface, and a comparative picture for HMX which will be evoked further on.**

## 3.0 Condensed Phase Processes

*The preheated zone* of a regressing propellant is described by the conservation of energy in a coordinate (x > 0 in the gas phase) regressing with the surface:

$$\rho_p \, v_b \, c_p \, dT / dx = d( \lambda_p \, dT / dx ) / dx \qquad (1)$$

in such a way that a temperature profile

$$( T - T_0 ) / ( T_s - T_0 ) = \exp( x \, v_b / d_p ), \; d_p \equiv \lambda_p / \rho_p \, c_p \qquad (2)$$

will progress with the surface into the propellant. From measurements up to 100°C and from ignition experiments, representative average values are taken as indicated in Table 3.

**Table 3: Values of the Condensed Phase Properties (Double-Base Propellants)**

| |
|---|
| $\rho_p = 1.6$ g/cm$^3$, $c_p = 0.4$ cal/g K, |
| $\lambda_p = 5.1 \; 10^{-4}$ cal/s cm K |
| $d_p = 0.8 \; 10^{-3}$ cm$^2$/s |

The thickness $e_{cond.}$ of the conduction zone can be taken conventionally as

$$T( \text{end of cond. zone} ) - T_0 = 10^{-2} ( T_s - T_o )$$

$$e_{cond.} = ( d_p / v_b ) \ln 10^2 \qquad (3)$$

As an example, for $v_b = 10$ mm/s

$e_{cond.} = 37 \mu$m, a thickness through which the temperature rises from 293 K to about 700 K. The residence time through this conduction zone is:

$$\tau_{cond.} = ( d_p / v_b^2 ) \ln 10^2 \qquad (4)$$

about 4 ms in this example; a very short time for a temperature increase of 400 K.

The *superficial degradation zone* has its thickness ruled by the conservation of the non degraded propellant mass fraction $Y_p$:

$$\rho_p \, v_b \, dY_p / dx = - \rho_p \, A_c \exp( - E_c / R \, T ), \qquad (5)$$

with the decomposition represented by an Arrhenius law. Numerous investigations by thermogravimetry, differential scanning calorimetry, on nitrocellulose, nitroglycerin and other nitrate esters, as well as on double base propellants, and ignition studies [5] result in:

**Table 4: Values for the Condensed Phase Degradation Kinetics (Double-Base Propellants)**

| |
|---|
| Decomposition order 0, $A_c = 1 \; 10^{17}$ s$^{-1}$, $E_c = 40$ kcal/mole |

The thickness of the degradation layer is related to the fast drop in the degradation rate. When this rate is $10^{-2}$ that at the surface temperature, the lower limit of the reaction layer is conventionally reached:

$$\exp[ - \xi_c / ( 1 - \Delta T / T_s )] = 10^{-2} \exp( - \xi_c ), \qquad \xi_c \equiv E_c / R\, T_s$$

the temperature drop is then

$$\Delta T / T_s = 1 / ( 1 + \xi_c / \ln 10^2 ) \tag{6}$$

$\Delta T \simeq 100$ K for $T_s = 700$ K. Such a temperature drop inserted in Eq. (2) gives an estimation of the reaction layer thickness

$$e_{reaction} = - ( d_p / v_b ) \ln[ 1 - \Delta T / ( T_s - T_o ) ]$$

or taking into account the magnitude of the reduced activation energy ( $\xi_c \approx 30$ ).

$$e_{reaction} \approx e_{cond.}\, T_s / \xi_c ( T_s - T_o ) \tag{7}$$

For the values taken above, at $v_b = 10$ mm/s, $e_{react} \approx 2$ μm, with an associated residence time $\tau_{react}$ of 0.2 ms.

The summation of Eq. (5) through the degradation layer results in:

$$\rho_p v_b ( Y_{p,s} - Y_{p,0} ) = - \int \rho_p A_c \exp( - E_c / R\, T ) \, dx \tag{8}$$

$$v_b \sim A_c \exp( - E_c / R\, T_s ) \quad e_{reaction} = A_c \exp( - \xi_c ) ( d_p / v_b ) \ln 10^2 ( 1 / \xi_c ) [ T_s / ( T_s - T_0 ) ]$$

A more rigorous approach [8] (which is almost identical to a numerical computation [9]) gives, for a zero order reaction:

$$v_b^2 = ( d_p / \xi_c ) A_c \exp( - \xi_c ) / ( 1 - T_0 / T_s - Q_s / 2\, c_p\, T_s ) \tag{9}$$

This equation indicates a relation between surface temperature and burning rate: the mass flow rate $\rho_p\, v_b$ emitted from the surface is the result of the decomposition of the propellant into gases throughout the superficial degradation layer, Eq. (8). The higher the burning rate $v_b$, the smaller the residence time $\tau_{react.} \sim 1 / v_b^2$, and the higher is the surface temperature reached to allow for the complete degradation of the propellant.

Traverses with micro-thermocouples (as seen previously the thickness of the combustion wave is of the order of tens of μm) allow to obtain measurements of the surface temperature [2,3,4,5]. One example is given on Fig. 6. The results from various sources are collected (see [5] for references), as burning rate versus $1 / T_s$, on Fig. 7. Also indicated is the correlation obtained from Eq. (9). Due to the thinness of the conduction zone, a few tens of micrometers, fairly large errors and scatter should be expected in the measurements of the surface temperature. Nevertheless, some conclusions can be reached (see also Refs. [3,10]). The initial degradation of the propellant components is controlled by the breaking of the -C-O-//-$NO_2$ bond (characterized by the 40 kcal/mole activation energy). This is considered to be a temperature sensitive only process, irreversible (therefore not influenced by the pressure level). It is noteworthy that the kinetics of the degradation is the same from thermal decomposition (by TG and DSC) at about 400 K, to ignition from 400 to 500 K [5] and combustion at temperatures up to 700 K. Also important is the conclusion, if one looks at the details of Fig. 7, that the presence of super rate producing additives does not affect the condensed phase kinetics.

*The energetics of the reaction layer* is now to be considered. The initial degradation of the propellant, taking into account the assumed decomposition of nitroglycerin into $3N0_2$, 2 $CH_2O$ and 0.5 $(CHO)_2$, is thought to give (for the example of the 1100 cal/g propellant) the mass balance

$$1 \text{ propellant} \rightarrow 0.467\ NO_2 + 0.364\ CH_2O + 0.1\ (CH0)_2 + 0.06 \text{ hydrocarbons} \qquad (10)$$

with a corresponding endothermic heat of degradation

$Q_d$ = - 135 cal/g of propellant.

It is thought [5,9,10] that within the superficial layer the exothermic reaction between $NO_2$ and aldehydes can start. A plausible mole balance (in order to match various results, in particular the analysis [7] of the gases emitted from the surface of regressing propellants) is

$$NO_2 + CH_2O \rightarrow NO + 1/2\ CO + 1/2\ CO_2 + 1/2\ H_2O + 1/2\ H_2 \qquad (11)$$

with a corresponding exothermic heat of reaction

$Q_{NO2}$ = 1040 cal/g of $NO_2$.

Conservation of the species $NO_2$ (in terms of mass fraction Y) is written (no diffusion is taken into account)

$$\rho_p\, v_b\, dY_{NO2} / dx = Y_{NO2,i}\, \rho_p\, A_c \exp( - E_c / R\, T ) - A_{NO2} ( p\, M / R\, T )\, Y_{NO2} \exp( - E_{NO2} / R\, T ) \qquad (12)$$

if a first order reaction with respect to the molar concentration of $NO_2$ is assumed (it will be seen that this is probably the case).

The conservation of energy is written

$$\rho_p\, v_b\, c\, dT / dx - d( \lambda\, dT / dx ) / dx = - Q_d\, \omega_p - Q_{NO2}\, \omega_{NO2} \qquad (13)$$

with $\omega_p$ the rate of reaction of the propellant, as in Eq. (5), and $\omega_{NO2}$ that of $NO_2$ as in the second term of Eq. (12). The summation of Eqs. (5,12,13) through the condensed phase to the surface leads to:

$$\lambda\, dT / dx|_s = \rho_p\, v_b ( c_g\, T_s - c_p\, T_o - Q_s ) \equiv \rho_p\, v_b\, Q_c \qquad (14)$$

$$Q_s \equiv Q_d + Q_{NO2} ( Y_{NO2,i} - Y_{NO2,s} ) \qquad (15)$$

The first equation is the heat balance at the surface, it means that the heat flux from the flame in the gas phase allows the heating and pyrolysis of the propellant. The net heat of decomposition of the propellant $Q_s$ is exothermic to the extent that some $NO_2$ already reacts exothermically in the condensed phase.

From thermocouple traverses such as that of Fig. 6 and the balance of Eq. (14), the net heat $Q_s$ can be estimated (again scatter should be expected). The results from various sources are given on Fig. 8. The net heat of decomposition is seen to be exothermic and increasing with burning rate (due to an increase in pressure). Summation of Eq. (12) yields (with Eq. (5) taken into account)

$$\rho_p\, v_b ( Y_{NO2,i} - Y_{NO2,s} ) = A_{NO2} \int ( p\, M / R\, T )\, Y_{NO2} \exp( - E_{NO2} / R\, T )\, dx$$

$$\approx A_{NO2} ( p\, M / R\, T_s )\, Y_{NO2} \exp( - E_{NO2} / R\, T_s )\, e_{react.}$$

and with Eq. (8)

$$Y_{NO2,i} - Y_{NO2,s} \sim ( p\, M / R\, T_s ) \exp( - E_{NO2} / R\, T_S ) / \exp( - E_c / R\, T_s )$$

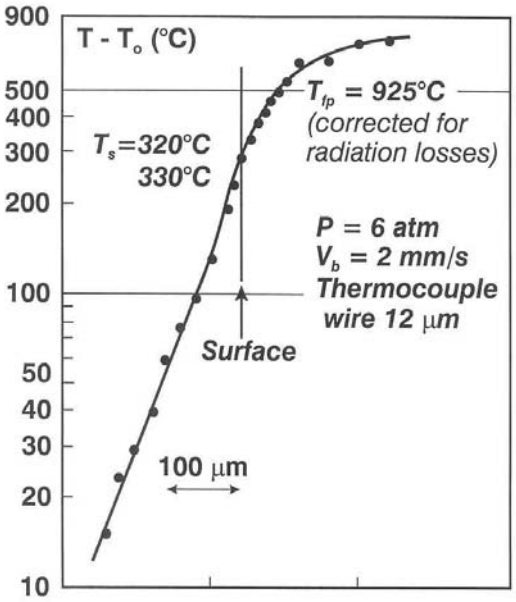


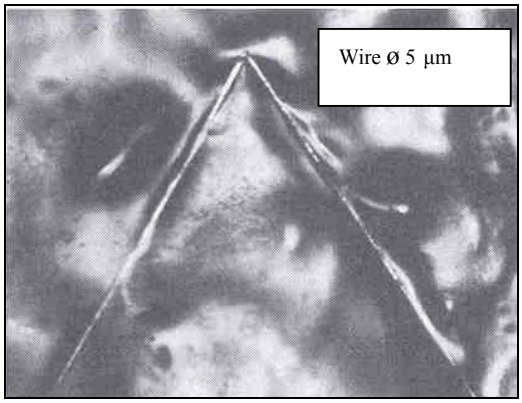


**Example of thermocouple**
**Pt – Pt / Rh soldered end to end**

**Figure 6: Temperature Profile in the Condensed Phase.**
**(Double Base Propellant)**

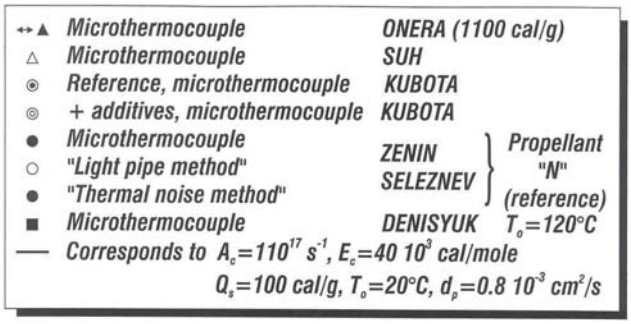


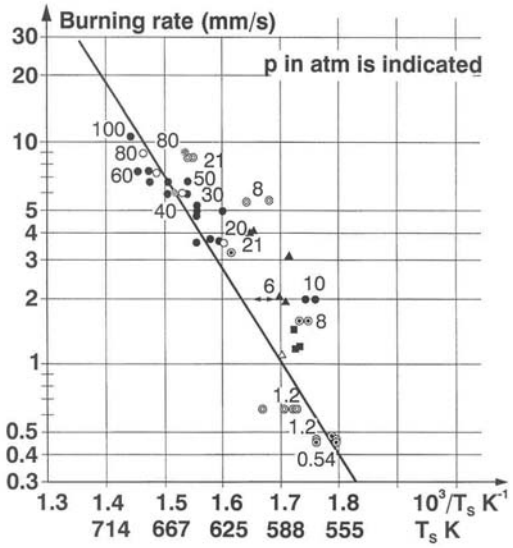


**Figure 7: Pyrolysis Law.**
**(Double Base Propellants)**

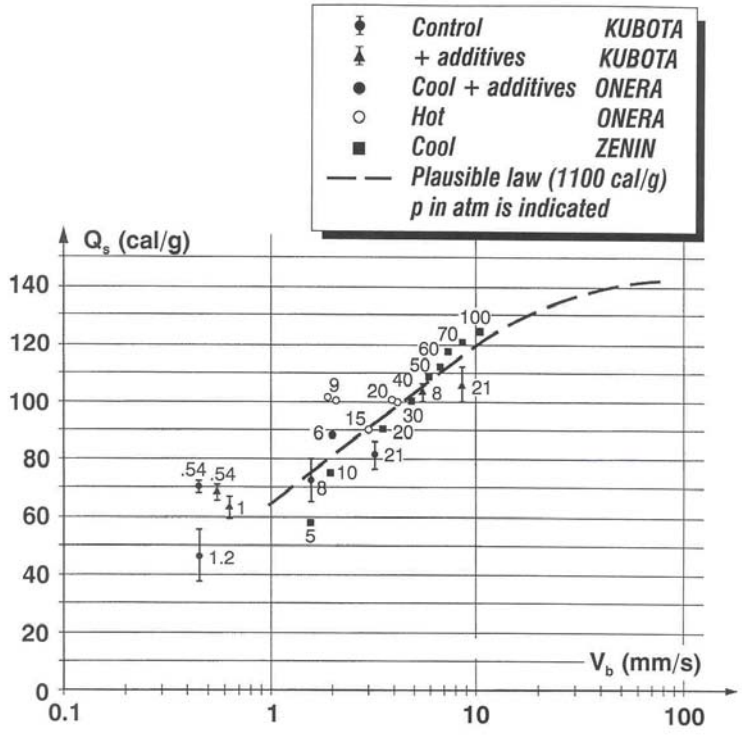


**Figure 8: Heat Evolved in the Condensed Phase.**
**(Double Base Propellants)**

This relation indicates that the amount of $NO_2$ reacting in the condensed phase will increase with pressure, and thus $Q_s$ will increase, if the reaction rate for $NO_2$ catches up with the decreasing residence time in the degradation layer,

$$\tau_{react.} \sim 1 / v_b^2 \sim 1 / \exp( - E_c / R T_s )$$

(due to Eq. (9)). A plausible law is obtained for a first order $NO_2$ reaction with an activation energy $E_{NO2}$ of about 15 kcal/mole.

It should be observed that the heat evolved in the condensed phase $Q_s$ has to be affected by the amount of $NO_2$ present in the propellant, that is by the heat of explosion.

One important feature of Fig. 8 is that the heat evolved in the condensed phase is not affected by the presence of additives.

## 4.0 Flame Zone

As seen above, the reaction between $NO_2$ and aldehyde starts in the condensed phase in such a way that the surface gas composition [7] indicated on Fig. 5 is obtained, with $NO_2$ being significantly less (0.255) as compared to what results from the initial degradation of the propellant (0.467, in the case of an 1100 cal/g propellant) and with NO already present (0.14). The mole balance of Eq. (11) allows to match as well the gas analysis at the end of the primary flame ([7], measurements at 11 atm)

$$NO_2 + CH_2O \rightarrow NO + 1/2\ CO + 1/2\ CO_2 + 1/2\ H_2O + 1/2\ H_2 \qquad (11)$$

$Q_{NO2}$ = 1040 cal/g of $NO_2$.

It is likely that aldehyde-aldehyde reactions also occur following (again to match the gas analysis results):

$$CH_2O + CH_2O \rightarrow CO + 1/2\ C_2H_4 + H_2O\ , \quad Q_{ald.1} = 389\ \text{cal/g of}\ CH_2O \tag{16}$$

$$(CHO)_2 + (CHO)_2 \rightarrow 4\ CO + 2\ H_2\ , \quad Q_{ald.2} = -\ 533\ \text{cal/g of}\ (CHO)_2 \tag{17}$$

At low pressure when probably only the reaction of (11) can take place, an energy balance between initial temperature and end of the primary flame yield:

$$c_g\ T_{fp} - c_p\ T_0 = Q_d + Q_{NO2}\ Y_{NO2,i},\ p \leq 1\ \text{atm} \tag{18}$$

since the initial $NO_2$ is totally consumed in the condensed phase and the primary flame. An evaluation of $T_{fp}$ = 1340 K results. It is seen on Fig. 9 that measurements with small thermocouples indicate a large increase with pressure of the primary flame temperature from this value. The aldehyde reactions of Eqs. (16,17) do not produce energy in significant amount. It is assumed [5] that the NO already present at the surface as well as that produced from the $NO_2$-aldehyde reaction react with the layer of carbon residue, attached to the surface, which is observed by direct visualization under combustion and after extinction by scanning electron microscopy.

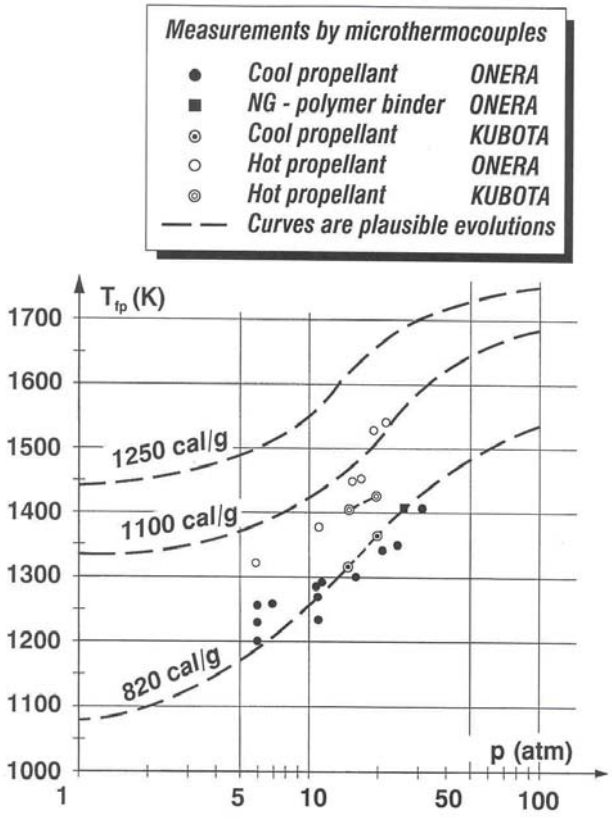


**Figure 9: Primary Flame Temperature of Double Base Propellants.**

The NO/carbon reaction had been investigated in [11]. If one makes use of the results obtained, the conservation of the species carbon can be written as (knowing that the carbon layer regresses with the surface)

$$v_b\ d\rho_c / dx = (\ M_c / M_{NO}\ )\ \omega_{NO} \tag{19}$$

$\omega_{NO} = - A_{NO/C} \exp( - E_{NO/C} / R T ) \rho_c S_{s,c} Y_{NO} p M$ , in g/cm$^3$s

(this form resulting from the way the data of [11] is cast), the reaction balance being assumed to be:

$NO + C \rightarrow 1/2\ N_2 + CO$ , $Q_{NO/C} = 1600$ cal/g of NO (20)

and $S_{s,c}$ being the specific surface area of the carbon (at most $10^6$ cm$^2$ /g). Reference [11] produces (after rounding $E_{NO/C}$)

$A_{NO/C} = 2\ 10^{-3}$ mole/s cm$^2$ atm, $E_{NO/C} = 30$ kcal/mole

A rough estimate of the amount of $N_2$ produced by reaction (20) through the primary flame is given by (with $m \equiv \rho_p v_b$ the mass flow rate)

$m Y_{N2,fp} = - ( 1 / 2 ) ( M_c / M_{NO} ) <\omega_{NO}> x_f$

$<\omega_{NO}>$ being evaluated at average values through the flame. With p = 11 atm, $v_b$ = 0.28 cm/s, $<Y_{NO}> = 0.2$, $<\rho_c> = 0.5$ g/cm$^3$, $<T_f>= 1400$ K and $x_f = 400$ µm (from thermocouple measurements) it is obtained

$Y_{N2,fp} \approx 0.06$

a reasonable value (with respect to the result of Fig. 5). This tends to indicate that the NO/carbon reaction has a kinetics indeed fast enough with respect to the residence time allowed in the primary flame.

An energy balance taking into account the NO/carbon reaction is written:

$c_g T_{fp} - c_p T_0 = Q_d + Q_{NO2} Y_{NO2,i} + Y_{NO,cons.} Q_{NO/C} + Q_{ald} Y_{ald,cons.}$ (21)

(the consideration of the aldehyde reaction cools the flame by about 80 K). In this balance $Y_{NO,cons.}$ is the amount of NO consumed in the primary flame:

$Y_{NO,cons.} = Y_{NO2,i} ( M_{NO} / M_{NO2} ) - Y_{NO,fp}$

in the case of the example of Fig. 5 and taking into account the uncertainty on the measurements: $Y_{NO,cons.} = 0.035$ to 0.047 and Eq. (21) results in $T_{fp} = 1420$ to 1475 K, an admissible value when compared to the results of Fig. 9.

The temperature profile in *the primary flame* is controlled by the conservation of energy [5].

$m c_g dT / dx - d(\lambda_g dT / dx) / dx = - Q_{NO2} \omega_{NO2} - Q_{NO/C} \omega_{NO} - Q_{ald} \omega_{ald.}$ (22)

**Table 5: Values Considered as Representative for the Gas Phase (Double-Base Propellants)**

| |
|---|
| $c_g = 0.35$ cal/g K, |
| $\lambda_g = 1.25\ 10^{-4} ( T / 700 )^{0.7}$ cal/cm s K |
| M = 30 g/mole |

The evaluation of the heat flux received at the surface, which will then control the burning rate according to Eq. (14), results from the summation of Eq. (22) through the flame zone. Only a true numerical evaluation of the temperature and species profiles will give the proper heat flux. However conclusions can be drawn from approximate relations. The activation energies of the reactions of Eq. (22) being moderate, the flame is distributed and an approximation of the temperature profile is written as:

$$( T_f - T ) / ( T_f - T_s ) = \exp( - 3 x / x_f ) \tag{23}$$

which will produce a shape such as that of Fig. 6. The coefficient of 3 is such that, when $x = x_f$, $T_f - T$ is 5 % of $T_f - T_s$, that is close enough to the final temperature.

With Eq. (14)

$$\lambda_{g,s} \, dT / dx|_s \equiv q_s = m \, Q_c \equiv \rho_p \, v_b \, (c_g \, T_s - c_p \, T_0 - Q_s) \tag{14}$$

Eq. (23) yields

$$q_s = 3 \, \lambda_{g,s} ( T_f - T_s ) / x_f , \qquad x_f = 3 \, \lambda_{g,s} ( T_f - T_s ) / m \, Q_c \tag{24}$$

The summation of Eq. (22) through the flame results in

$m \, c_g ( T_f - T_s ) + q_s = 3 \, Q_g <\omega_g> x_f$ ($<\omega_g>$ positive is the average rate)

or with Eqs. (14,24), and taking into account an overall equation for conservation of energy

$c_g ( T_f - T_s ) = Q_g - Q_c$,

$$m = [3 <\omega_g> \lambda_{g,s} ( T_f - T_s ) / Q_c]^{1/2} \tag{25}$$

At very low pressure, ≈ 1 atm, when only the $NO_2$ reaction probably takes place, the burning rate follows pressure according to, see Eq. (12),

$$m \equiv \rho_p \, v_b \sim ( <\omega_{NO2}> )^{1/2} \sim p^{1/2} \exp( - E_{NO2} / 2 \, R \, T_{fp} ) \tag{26}$$

a pressure exponent which is indeed observed, see Fig. 2. As the pressure increases the NO/carbon reaction takes on more importance and, referring to Eq. (19),

$$m \equiv \rho_p \, v_b \sim [ p \exp( - E_{NO2} / R \, T_{fp} ) + \sim p \exp( - E_{NO/C} / R \, T_{fp} ) ]^{1/2}, \tag{27}$$

which, with the increase of the flame temperature with pressure, see Fig. 9, accounts for the pressure exponent of 0.7.

At higher pressures, above about 150 atm for the 1100 cal/g propellant for example, a change in the pressure sensitivity, Fig. 2 is observed. This tends to indicate that *the secondary flame*, probably characterized by a second order, with respect to pressure, reaction for NO, comes into the primary flame and progressively dominates it, with a pressure exponent, according to Eq. (25), increasing to close to 1.

Referring to Fig. 10, for the 1250 cal/g propellant, the temperature sensitivity is indicated:

$$\sigma_p = ( d \ln v_b / dT_o ) \text{ at p given} \tag{28}$$

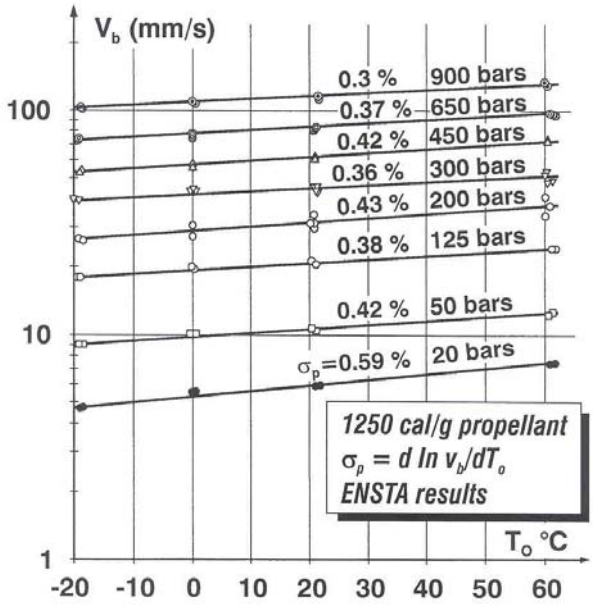


**Figure 10: Temperature Sensitivity of a Double Base Propellant.**

According to Eq. (27) the burning rate is under the influence (noting that the condensed phase energy balance also contains the effect of $T_0$ see Eq. (14)) of a premixed flame heat flux and therefore very sensitive to changes in the primary flame temperature, in the pressure domain when the two flames are separated. From Eq. (21), any change in initial temperature will affect the primary flame temperature and therefore induce a change in burning rate. As the pressure rises the primary flame temperature increases (up to 1800 K) and then for higher pressures the burning rate comes under the influence of the final flame (with a temperature reaching 3110 K for the 1250 cal/g propellant). It is seen from Eq. (27) that a given change in $T_0$ and therefore in $T_f$ has a smaller impact on the burning rate for higher flame temperatures, that is for higher pressures, a tendency observed on Fig. 10.

## 5.0 Active Binders

Various types of active binders, based on nitrocellulose or an inert binder and nitroglycerin or less energetic liquid nitrates, can be used, see reference [10] for a complete description. The cross-linked double-base binders (XLDB) will be considered here, in which the polymer is cured with an isocyanate after mixing with NG.

**Table 6: Values for a XLDB Binder**

| |
|---|
| Composition: ≈ 2/3 NG, 1/3 polyethylene glycol. |
| Heat of explosion: 850 cal/g. |
| $T_{ff}$ = 2000 K. $\rho_p$ = 1.42 g/cm$^3$. |
| $c_p$ = 0.46 cal/g K. |
| $\lambda_p$ = 3.9 $10^{-4}$ cal/cm s K. $d_p$ = 0.6 $10^{-3}$ cm$^2$/s |
| $Y_{NO2,i}$ = 0.421. $Q_d$ = - 150 cal/g |

Although the burning rates of the different active binders can be, for a given heat of explosion, somewhat different at low pressures [10], above 10 atm the differences become small , see Fig. 11. In the case of a double-base propellant and of a XLDB binder (that of the above table), with nearly the same heat of explosion, the burning rates for a large range of pressure are very close, Fig. 12.

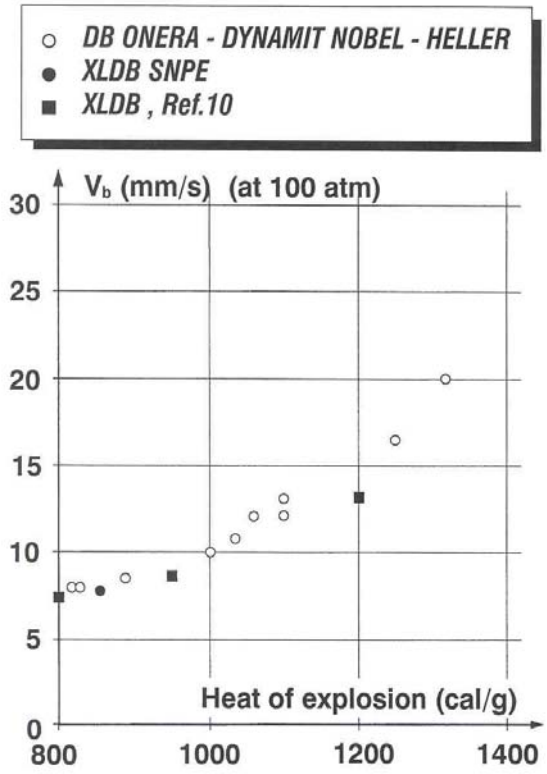


**Figure 11: Burning Rate vs Heat of Explosion.**
**(Double Base Propellants and XLDB Binders)**

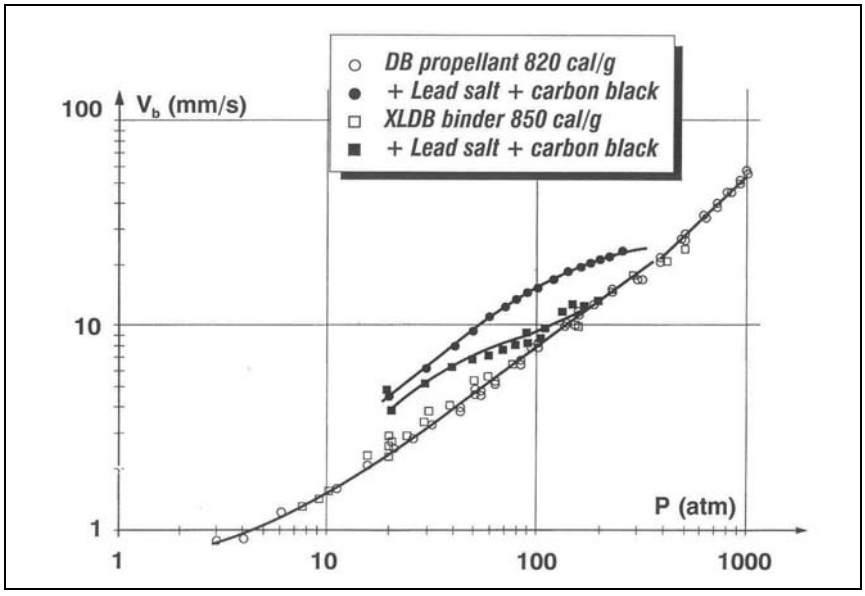


**Figure 12: Double Base Propellants and Active Binder Burning Rates.**

Measurements for XLDB binders of the degradation kinetics, of the surface temperature, of the heat evolved in the condensed phase, as in Fig. 8, and of the primary flame temperature, Fig. 9, show that these characteristics are very close to those of DB propellants.

**Table 7: Gases Evolved from the Surface, Mass Fractions. XLDB Binder [7]**

| $NO_2$ | $CH_2O$ | $(CHO)_2$ | NO | CO | $CO_2$ | $H_2O$ | HC |
|---|---|---|---|---|---|---|---|
| 0.31 | 0.37 | 0.08 | 0.07 | 0.03 | 0.04 | 0.02 | 0.08 |

Gas analysis at the surface gives results which are qualitatively comparable to those of DB propellants, Fig. 5.

It can then be stated that the combustion mechanisms of the various types of double-base propellants and of the active binders are very similar.

## 6.0 Mechanisms of Action of Additives

The incorporation of a few per-cents of lead (and copper) salts and carbon black enables to obtain super-rate effects followed by mesa or plateau effects in the burning rate versus pressure laws of double-base propellants, Fig. 3, as well as of active binders, Fig. 12, although in the latter case these effects are much less pronounced.

What is thought to be the mechanism of action of the additives has been presented in references [5,6] by the authors and in reference [12].

It has been found that the active part of the lead salt is the oxide of lead which accumulates above the propellant surface, after the salt has been trapped in the carbon residue layer which can be observed, immersed in the primary flame (the decomposition kinetics of the salt is slower than that of the propellant components and it thus emerges from the surface unchanged). If the propellant (when its heat of explosion increases) or the active binder naturally produces less carbon residue, then the lead salt particles are in large part ejected from the surface and cannot act. This is the case probably when the amount of nitrocellulose is reduced (hot double-base propellants) or almost absent (XLDB binders). In the latter case however the inert polymer leaves some carbonaceous residue. Addition of carbon black is probably favorable because it accumulates on the surface in the naturally produced carbon layer.

It has been found by the authors that PbO reacts preferentially with aldehydes to form carbon and $CO_2$. It has been observed systematically [6] that there is a relation between the amount of carbon residue and the importance of the super-rate observed (for example, depending on the fabrication process: solventless extrusion, powder casting, mixing). It was seen that the primary flame is due to an $NO_2$-aldehyde reaction. But NO starts to react with carbon as well close to the surface, leading to the increase in primary flame temperature of Fig. 9. It is believed that the extra carbon produced in the presence of additives enhances the NO/C reaction (see ref. [12] for more results on this reaction), depositing extra energy in the primary flame (an increase in primary flame temperature is observed in the presence of additives [5]) and resulting in a higher heat flux to the surface, and thus a higher burning rate.

Figure 13 shows surface structures of a cool propellant with a strong super-rate and a corresponding thick carbon residue. In this case, visualization shows that a physical effect occurs in which the secondary luminous flame attaches in streaks to the carbon layer and deposits its high temperature ($\approx$ 2200 K as compared to the $\approx$ 1400 K of the primary flame) closer to the surface. The abrupt end of the super-rate,

the mesa effect, is believed to be due to the too thick carbon residue being expelled from the surface. At the end of the mesa effect the surface is almost clean of carbon.

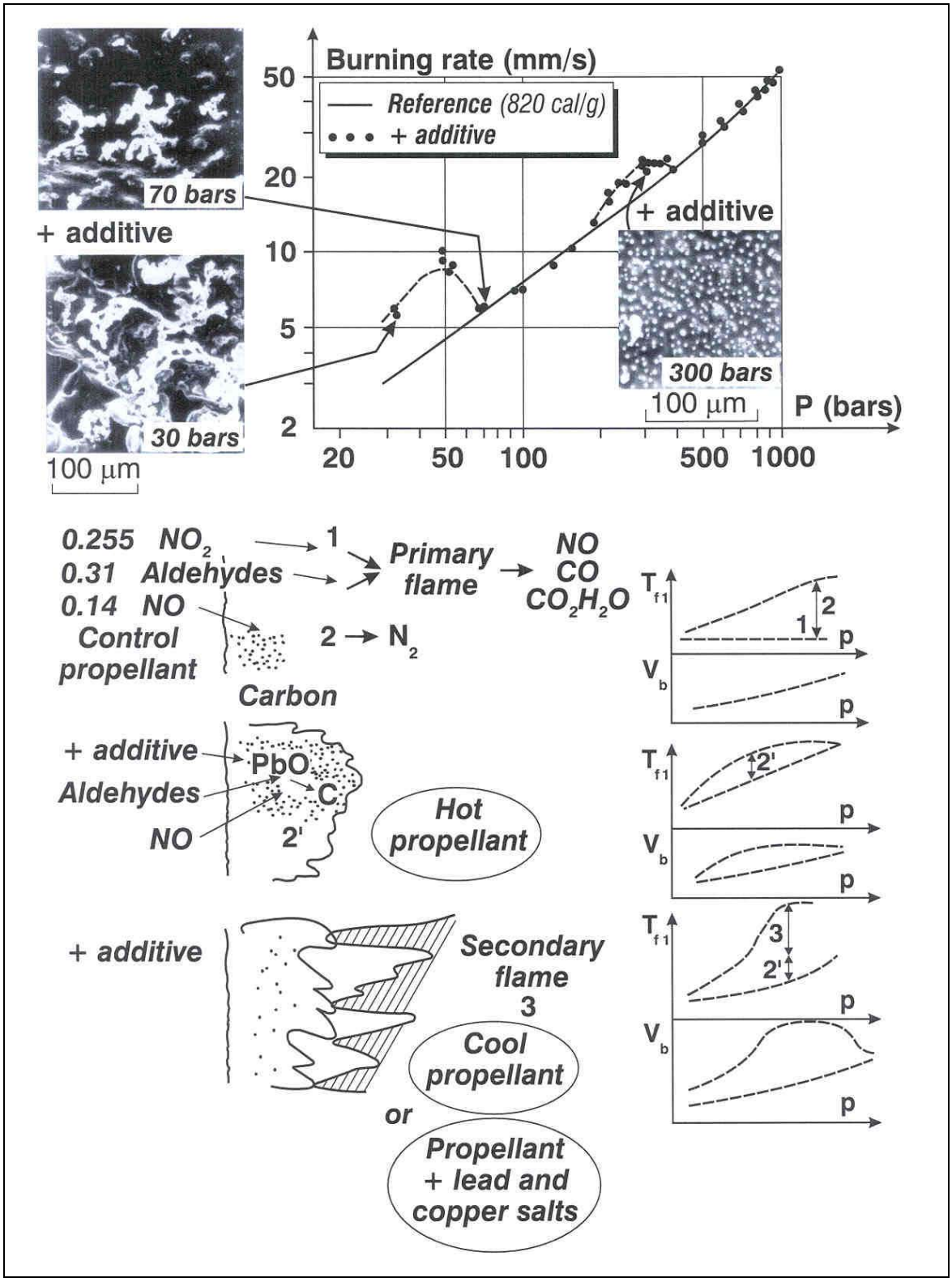


**Figure 13: Super Rate Effects in Double Base Propellants.**

In the case of hot propellants, Fig. 3, the super-rate is probably due only to the chemical effect of the enhanced NO/C reaction. As the pressure increases the secondary flame, where NO will react anyway, merges into the primary flame and progressively the modified propellant is caught up by the reference propellant, a plateau effect thus resulting.

In the high pressure domain when the flame system has reduced to one overall flame, a second super-rate occurs (when only lead salt or oxide is added), see Fig. 13 for the cool propellant and Fig. 3 for a 1250 cal/g propellant. This effect seems to be purely physical, related to the presence of lead oxide particles accumulating and imbedding into the surface, Fig. 13, with for example an enhancement of the thermal conductivity of the flame zone or more probably a flame holding effect (the protruding particles perturb the flow from the surface). At higher pressures and burning rates the thickness of the condensed phase heated zone and reaction layer and flame zone becomes so small that the particles will not attach to the surface or will be too large to perturb the combustion process.

## PYROLYSIS OF INERT BINDERS

A number of books and works has been devoted to the behavior of polymers, whether or not usable as binders, under thermal loads, references [13-17] are examples. Much work has been carried out with thermogravimetric analysis (TGA) or differential scanning calorimetry (DSC), with heating rates at most of the order of 1°C/s. Under linear pyrolysis (for a binder within a solid propellant) the rate of temperature increase is of the order of $10^5$ °C/s. It is far from obvious a priori that the degradation kinetics will remain the same. In Ref. [8] it was attempted to establish that this is indeed the case for a number of polymers.

Although it is hardly a propellant binder, Teflon is an interesting reference polymer. Its degradation kinetics (obtained by TGA) and thermal properties [8] ( $\lambda_p$ = 6.34 $10^{-4}$ cal/cm K s, $\rho_p$ = 2.1 g/cm$^3$, $c_p$ = 0.25 cal/g K) are indicated on Fig. 14. In order to extrapolate these characteristics to the regime of linear pyrolysis (obtained experimentally by pressing the sample on a hot plate) the procedure of reference [8], also explained in the condensed phase paragraph of the double-base propellants chapter, is applied. In the case of a first order (with respect to the non degraded polymer) reaction, the relation between regression rate and surface temperature is (again, numerical computation shows this relation to be accurate to about 1 %)

$$v_r^2 = ( d_p / \xi_c) A_c \exp( - \xi_c ) /[ ( - \ln Y_{p,s} ) ( 1 - T_0 / T_s - Q_s / c_p T_s ) + Q_s / c_p T_s ] \quad (1)$$

$$\xi_c \equiv E_c / R T_s$$

In this relation $Q_s$ is the heat evolved in the condensed phase, in this case endothermic and equal to - 340 cal/g ( $Y_{p,s}$ mass fraction of the remaining polymer at the surface can be set at 0.01 ). It is seen on Fig. 14 that there is a good match between extrapolated law and measurements. These measurements are obtained under various atmospheres, showing no influence of this factor. The conclusion is then reached that the pyrolysis of such a polymer is an irreversible thermal mechanism.

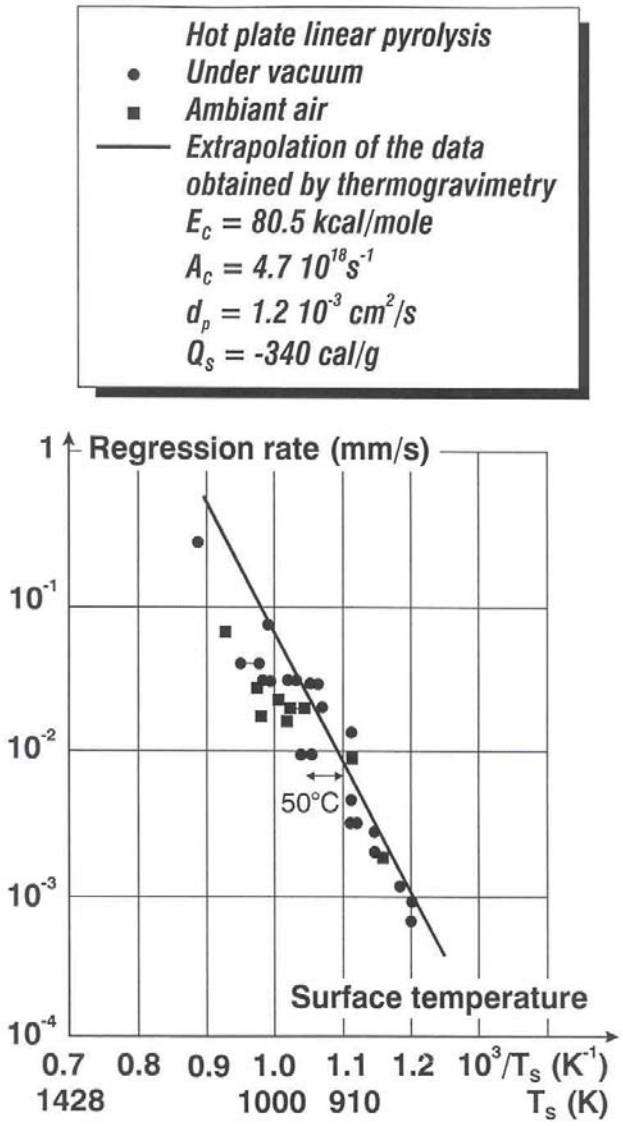


**Figure 14: Linear Pyrolysis and Extrapolation of Thermogravimetric Results (Example of Teflon).**

In the case of an actual, widely used, propellant binder such as hydroxyl terminated polybutadiene (HTPB) the same extrapolation can be made, Fig. 15 (the thermal properties used: $\lambda_p$ = 3.6 $10^{-4}$ cal/cm K s, $\rho_p$ = 0.92 g/$cm^3$, $c_p$ = 0.39 cal/g K), and compared to the results of Ref. [15], obtained in a hybrid motor, gaseous oxygen upon HTPB, with the surface temperature being measured by infra-red pyrometry (with some dispersion). A measurement obtained by the authors with $CO_2$ laser heating and IR pyrometer is also indicated. The agreement, considering the extent of the extrapolation, is very satisfactory. Further on, the pyrolysis law based on the TGA and DSC kinetics will be considered to apply.

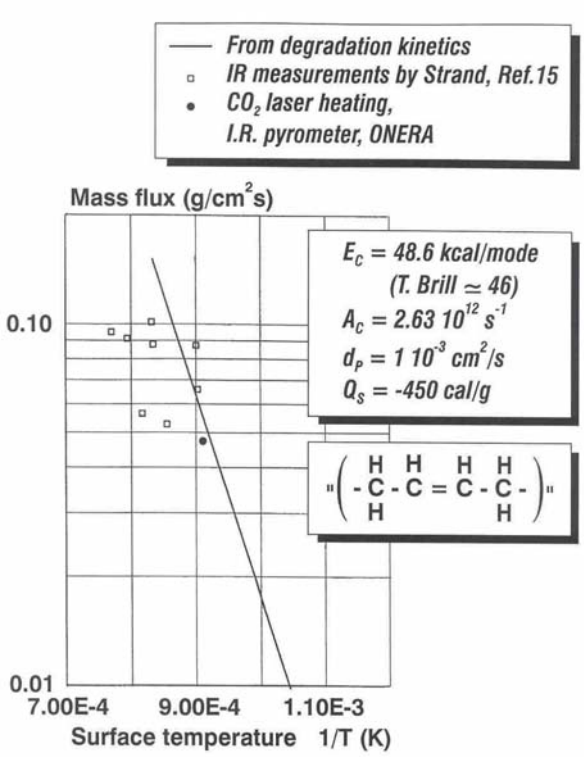


**Figure 15: Pyrolysis Law for HTPB.**

Equation (1) and Fig. 15 indicate how the surface temperature adjusts itself to allow the polymer to degrade into gases when the regression rate changes. Further considerations to better know the binder behavior are the nature of the gases resulting from the pyrolysis and the corresponding heat of degradation.

The heat of ablation of HTPB was measured in Ref. [16] by relating the mass ablated to the radiation heat flux received by a sample. For a regression rate of 0.4 mm/s (and from Fig. 15 $T_s \approx 1060$ K) it is obtained:

$$h_{abl} = c_p ( T_s - T_0 ) - Q_s = 750 \text{ cal/g}$$

$$Q_s = -450 \text{ cal/g}$$

It is found that this value is compatible with the production of mostly $C_4H_6$ as pyrolysis gas. Gas analysis at low temperature [13] reveals a complex set of gases (≈ 45 % in mass butadiene, ethylene, propene…) resulting from the degradation of HTPB. If one evaluates the difference in heats of formation between the initial material and butadiene it is found:

$$\Delta h = h^\circ (C_4 H_6 ) - h^\circ (\text{HTPB}) = 496 \text{ cal/g} - 5 \text{ cal/g} \approx 490 \text{ cal/g}$$

close to the measured heat of degradation. At high heating rates butadiene is probably the major degradation gas.

## COMBUSTION OF AMMONIUM PERCHLORATE

Ammonium perchlorate (AP), $NH_4\ ClO_4$, is a widely used oxidizer and as such has been the object of numerous investigations. References [18 to 22] are a sampling, with [22] giving a detailed list. A view of

the combustion of AP is presented herein attempting to make use as much as possible of the various experimental data available. Due to the large number of works on AP combustion, somewhat contradictory interpretations and corresponding models have been produced. A simplified model is presented, which is considered to represent reasonably the combustion mechanism of AP, although it will not be in agreement with all of the above mentioned interpretations.

## 1.0 Condensed Phase Behavior

The considerations presented previously for the condensed phase of a pyrolysing monopropellant apply to AP. The conduction zone has a thickness

$e_{cond.} = ( d_p / v_b ) \ln 10^2$

(with the thermal diffusivity [21] $d_p \approx 1.2\ 10^{-3}$ $cm^2/s$ at an average temperature in the heat wave), thus equal to ≈ 55 μm, for a burning rate of 10 mm/s.

**Table 8: Condensed Phase Values for AP [19,21]**

| |
|---|
| $c_p$ = 0.31 cal/g K (orthorhombic phase < 513 K) = 0.365 cal/g K (cubic phase) |
| $\rho_p$ = 1.95 g/$cm^3$ , $d_p = 2.5\ 10^{-3} - 4.55\ 10^{-6}$ T(°C)$cm^2/s$ |

Based on observations by scanning electron microscopy after extinction, the idea has been advanced that the self-deflagration of AP, possible only above 20 atm, requires that a large amount of exothermic reaction already takes place in the condensed phase in a thin liquid layer (above a melting temperature estimated at 835 K) [19,20,21,22].

## 2.0 Energetics of the AP Combustion

The model of Ref. [19] is subscribed to in order to describe the combustion of AP alone. The AP undergoes a phase transition at 513 K, melts around 830 K and, in the thin (a few microns) superficial liquid layer thus created, an exothermic reaction, affecting 70 % of the AP, takes place and creates the final combustion gases, $O_2$ in particular. The remaining 30 % of the AP sublime into $NH_3$ and $HClO_4$ which react exothermically in a premixed flame very close to the surface (a few microns), Fig. 16.

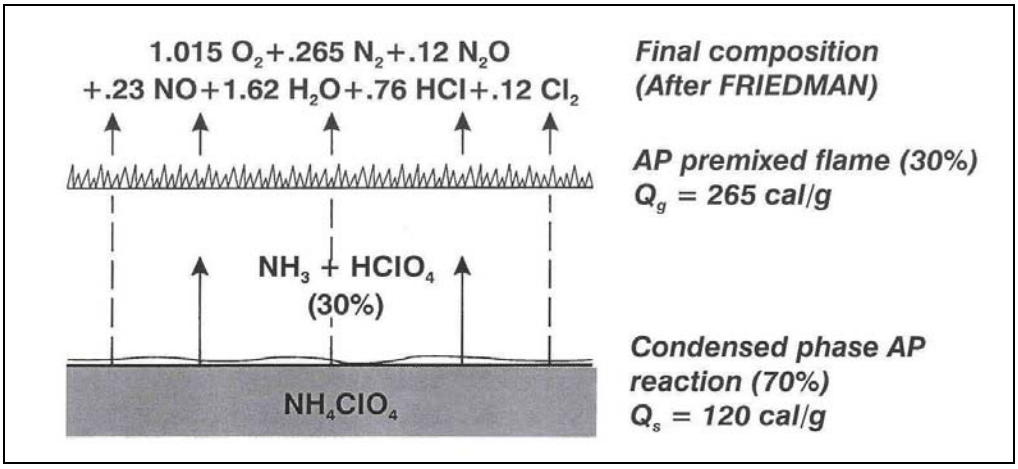


**Figure 16: Autonomous Combustion of Ammonium Perchlorate.**

From the data collected in [19] the change of enthalpy per gram of AP required to heat up the AP to its surface temperature, $T_{S,AP}$, is estimated as

$$\Delta h_{H,AP} = 0.31 ( 513 - 293 ) + 21 + 0.365 ( 835 - 513 ) + 60 + 0.328 ( T_{S,AP} - 830 ),$$
$$= 266 + 0.328 ( T_{S,AP} - 835 ) \text{ cal/g} \quad (1)$$

where the heat of transition and the heat of liquefaction appear. The exothermic condensed phase degradation involves an enthalpy change of [19]

$$\Delta h_{D,AP} \approx - 380 \text{ cal/gram of reacting AP.} \quad (2)$$

The heat of sublimation is 58 ∀ 2 kcal/mole or

$$\Delta h_{S,AP} = 476 \text{ to } 510 \text{ cal/gram of subliming AP.} \quad (3)$$

The adiabatic flame temperature for the combustion of AP alone has been estimated in [18] to be $T_{f,AP}^{ad} = 1205$ K, corresponding to the reaction

$$NH_4 ClO_4 \rightarrow 0.265 N_2 + 0.12 N_2O + 0.23 NO + 1.62 H_2O + 0.76 HCl + 0.12 Cl_2 + 1.015 O_2 \quad (4)$$

The change of enthalpy, $\Delta h_{C,AP}$, corresponding to the combustion of the sublimed $NH_3$ and $HClO_4$ (to give the combustion products of (4)) is obtained from the equation expressing the conservation of enthalpy between the unreacted AP at initial temperature and the combustion products downstream of the flame:

$$0.3 \Delta h_{C,AP} + c_g ( T_{f,AP}^{ad} - T_{S,AP} ) + 0.3 \Delta h_{S,AP} + 0.7 \Delta h_{D,AP} + \Delta h_{H,AP} = 0 \quad (5)$$

For $c_g \approx 0.3$, value taken in [19], it is found

$$\Delta h_{C,AP} = - 850 \text{ to } - 885 \text{ cal/gram of reacting AP,} \quad (6)$$

depending on the value adopted for the heat of sublimation, 476 or 510 cal/g, and independently of the value of $T_{S,AP}$ in the range found in [19].

It should be noticed that the value given here for the transformation of the AP into gases (that is $NH_3$ and $HClO_4$ for the subliming 30 % and the combustion gases of (4) for the 70 % reacting in the condensed phase), namely

$$- Q_s = 0.3 ( 476 \text{ to } 510 ) + 0.7 ( - 380 ) = - 123 \text{ to } - 113 \text{ cal/g of AP,} \quad (7)$$

is also found in [20], where a model for the combustion of AP similar to that of [19] is adopted. The heat evolved in the condensed phase $Q_s$ ( > 0 if exothermic) will be set equal to 120 cal/g.

One last check of consistency can be performed: with the enthalpy of formation of AP at $h^0_{AP} = - 602$ cal/g and that of the combustion products of (4) $h^0_{CP} = - 877$ cal/g, an overall energy balance between initial AP and combustion products is:

$$c_g T_{f,AP}^{ad} + h^0_{CP} = c_{ortho} T_0 + h^0_{AP} \quad (8)$$

resulting in $T_{f,AP}^{ad} = 1215$ K, close enough to the previous value.

## 3.0 Surface Pyrolysis of AP

Attempts to measure the surface temperature give values between 670 and 973 K. These results, obtained either by using thermocouples imbedded in the AP pellet, or by measuring the radiation emitted by the surface, are always associated with some uncertainty due to the operating methods. In effect, the large size of the thermocouples, in relation to the temperature gradients encountered, favors errors; further, the measurement represents an averaging of surrounding conditions. The temperatures thus obtained are therefore probably somewhat lower than in reality. In the case of experiments using an optical technique, the temperature is deduced from measuring the radiation emitted by the surface and transmitted through the gaseous layer. The disturbance caused by the radiation of the gases and the screening action of the flame limits the application of this method to 60 atm. That is why the original technique suggested by Seleznev [23], carried out by using a sapphire light guide inserted in the solid substance and by reading the infra-red emission in the direction of the condensed phase, has the considerable advantage of providing a direct measurement of the radiation emitted by the surface, without any hot gases and the reaction of the flame being interposed. Its application can therefore be extended to high pressures and the measurements appear to be more convincing. These results enable to determine the AP pyrolysis law.

Further, estimates of the AP melting temperature are mentioned by a number of authors; the values suggested vary from 715 to 865 ± 20 K and are useful in interpreting the extinction phenomenon at low pressure.

The pyrolysis law of the AP is written as:

$$m_{AP} = \rho_{AP}\, v_{b,AP} = A_{S,AP} \exp( - E_{S,AP} / R\, T_{S,AP} ) \qquad (9)$$

The parameters characterizing the pyrolysis law are determined so as to obtain a good agreement between the rates and the surface temperatures measured by Seleznev [23] (Fig. 17). The activation energy obtained is 20 kcal/mole, a figure compatible with the various estimates encountered. The measurement of the surface temperature made at 40 atm is the only one which deviates from that computed by the pyrolysis law used. On the other hand, for the critical rate of 0.27 cm/s obtained at 20 atm (AP combustion pressure limit), this law allows for a surface temperature of 830 K, corresponding to the assumed AP melting temperature [19].

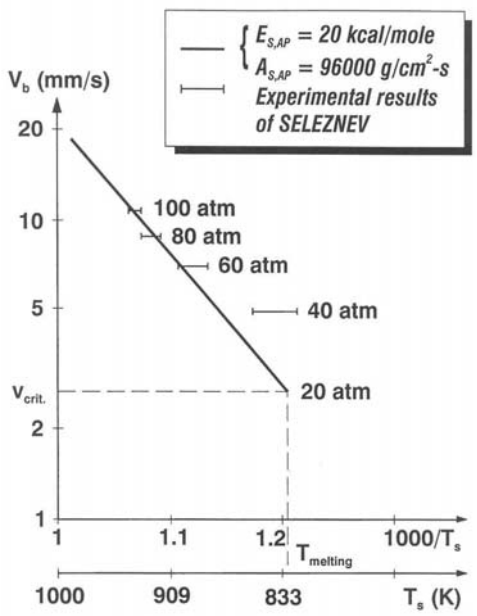


**Figure 17: Pyrolysis Law for Ammonium Perchlorate.**

## 4.0 Flame Structure of the AP Combustion

The approach of [19] considers 14 different reactions to describe the flame zone of the AP, involving 30 % of the material sublimed into $NH_3$ and $HClO_4$. An overall second order reaction is then obtained

$NH_3 + HClO_4 \rightarrow$ products of Eq. (4)

with an activation energy of $E_{g,AP} = 15$ kcal/mole.

A simplified model is constructed like the one used in the chapter on the double base flame. The temperature profile is approximated as

$$( T_{f,AP}^{ad} - T ) / ( T_{f,AP}^{ad} - T_{S,AP} ) = \exp( - 3 x / x_f ) \quad (10)$$

with the boundary condition

$$q_s \equiv \lambda_{g,s} \, dT / dx|_s = m_{AP} \, Q_c \quad (11)$$

$$Q_c = \Delta h_{H,AP} - Q_s$$

$Q_c$ is the heat required to bring the AP from $T_0$ to gases at the surface, see Eqs. (1) and (7).

Combining (10) and (11) results in

$$m_{AP} = 3 \lambda_{g,s} ( T_{f,AP}^{ad} - T_{S,AP} ) / x_f \, Q_c \quad (12)$$

Summation of the energy equation from $T_{s,AP}$, x = o, to $x_f$ yields, after using Eqs. (11) and (12) and Eq. (5) written as

$$Q_g + c_g ( T_{f,AP}^{ad} - T_{S,AP} ) + Q_c = 0$$

$$m_{AP} = [ 3 \langle \omega_g \rangle \lambda_{g,s} ( T_{f,AP}^{ad} - T_{S,AP} ) / Q_c ]^{1/2} \quad (13)$$

In this equation the average reaction rate is written as

$$3 \langle \omega_g \rangle = p^2 A_{g,AP} \exp( - E_{g,AP} / R \, T_{f,AP}^{ad} ) \quad (14)$$

expressing a second order overall rate. The burning rate is then found to follow pressure with an exponent close to 1. Table 9 indicates various values for AP combustion.

**Table 9: Values Considered as Representative for the AP Flame Zone**

| | |
|---|---|
| $\rho_{AP}$ | $= 1.95$ g/cm$^3$ |
| $E_{S,AP}$ | $= 20$ kcal/mole |
| $A_{S,AP}$ | $= 96000$ g/cm$^2$ s |
| $E_{g,AP}$ | $= 15$ kcal/mole |
| $A_{g,AP}$ | $= 700$ g/cm$^3$ s atm$^2$ |
| $\gamma$ | $= 30$ % |
| $c_g$ | $= 0.3$ cal/g K |
| $\lambda_g$ | $= 1.9 \, 10^{-4}$ cal/cm s K |

Taking into account the various values given, it is obtained for $v_b$ = 10 mm/s ( $T_{S,AP} \approx 925$ K ) the flame stand-off distance, Eq. (12), ( $Q_c$ = 175 cal/g ), $x_f \approx 5$ µm, the height to reach $T_f$ within 5 %.

The only input data which is not defined from outside considerations is the pre-exponential factor $A_{g,AP}$ used as a floating parameter for the model. Various numerical values associated with the input parameters of the model are brought together in the above table. Just by the choice of the prefactor $A_{g,AP}$ adjusted at 700 g/cm$^3$ s atm$^2$, the model satisfactorily reproduces variations in the AP burning rate due to pressure as well as due to the change in the initial temperature of the product. Figure 18 provides a comparison of computed rate curves with experimental points [21].

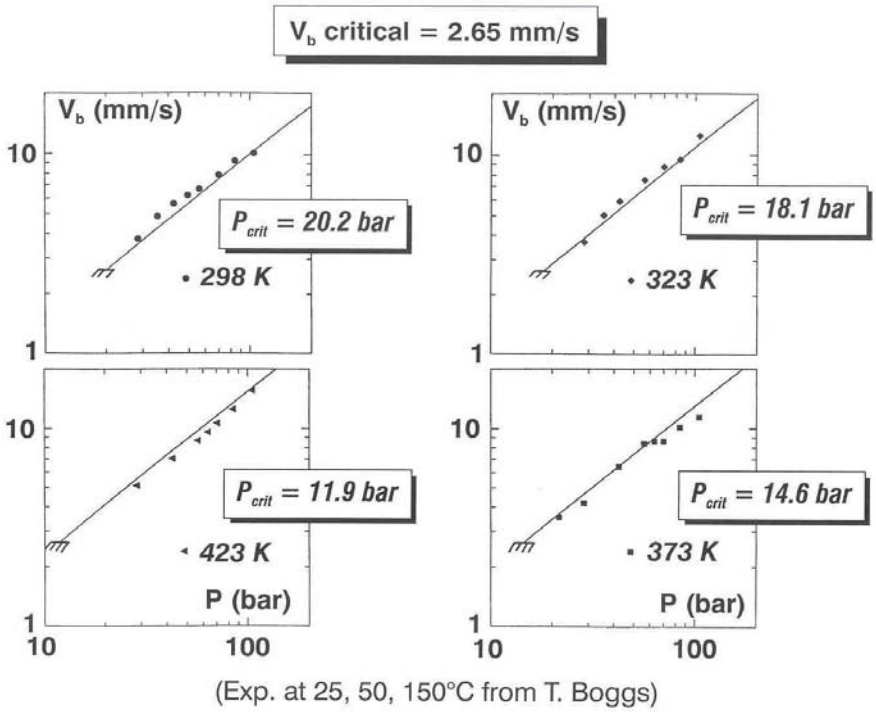


**Figure 18: Burning Rate of Ammonium Perchlorate at Different Initial Temperatures.**

At sufficiently high pressures, the energy transmitted from the flame toward the surface, to which must be added the effect of the superficial exothermic reactions, maintains the surface temperature above the AP melting point. When the pressure falls, the premixed flame moves away and the surface temperature can then drop below the limiting value, thus causing the disappearance of the liquid surface layer which was enabling the exothermic reactions to occur. The energy from the flame is then much too small to maintain a pyrolysis which has become strongly endothermic and AP no longer burns. This minimum pressure, beyond which the combustion cannot propagate itself, sets the pressure limit for AP self-degradation.

On the basis of this hypothesis, the combustion pressure limit is reached when the surface temperature is equal to the AP melting temperature. It is interesting to use the model in order to follow the variation of the computed limiting pressure with the initial temperature. At atmospheric temperature, the combustion limit is 20 atm, in agreement with experimental results. The critical rate of 0.27 cm/s and the surface temperature of 830 K, representing the AP melting temperature, corresponds to it. The computation method consists, for the initial temperature varying between 0 and 200°C, in finding for what pressure the surface temperature is equal to 830 K. A comparison between the computed and experimental pressure limits is very good, Fig. 19, and confirms the soundness of the hypothesis following which AP only burns if the surface temperature exceeds its melting temperature.

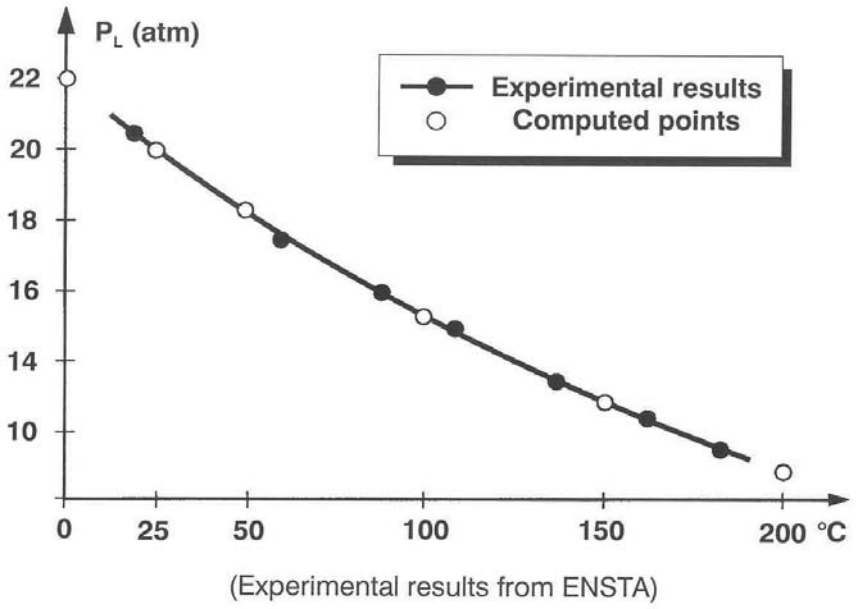


**Figure 19: Limiting Pressure for Combustion of Ammonium Perchlorate.**

One further set of results is presented. Questions have been raised about the combustion of AP at high pressures, above about 100 atm, with many conflicting results. Measurements of burning rates on carefully inhibited samples are presented on Fig. 20. It is concluded that no strong change of combustion regime is observed. The model based on the above presented hypothesis seem to follow quite well the results to high pressures.

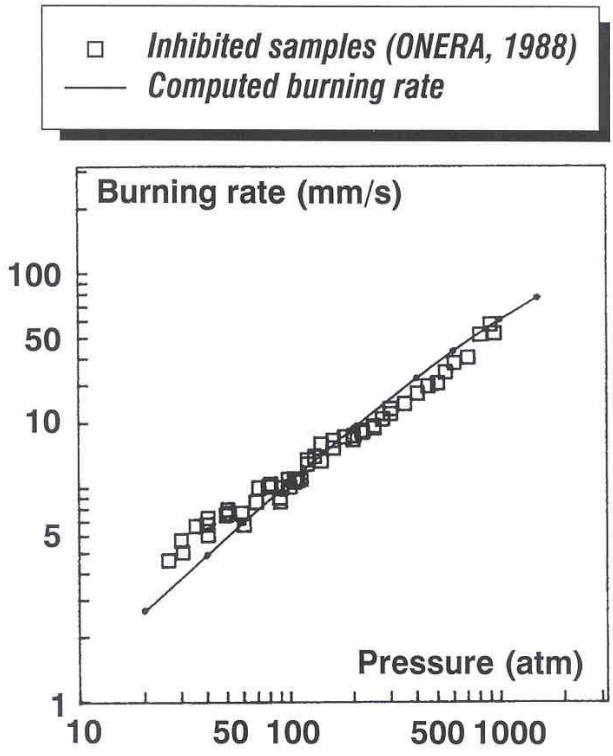


**Figure 20: Burning Rate of Ammonium Perchlorate at High Pressures.**

# COMBUSTION OF HMX

The combustion of HMX, which has balanced oxidizing and combustible elements (to reach CO, $H_2O$ and $N_2$) and a combustion temperature of 3280 K, is controlled by processes in the condensed phase as well as in the flame zone. Information about these processes is to be found in references [24 to 31] (also [21]).

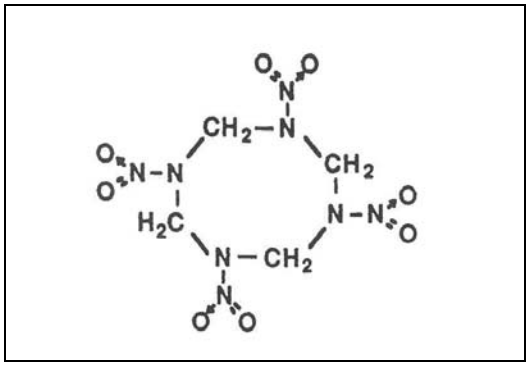

**Figure 21: Chemical Structure of HMX.**

## 1.0 Condensed Phase Processes

The kinetics of the decomposition of HMX can be obtained by differential thermal analysis [24,29]. A fairly extensive review is given in Ref. [25]. Results obtained around the (assumed) melting temperature of 556 K are indicated on Fig. 22, with the kinetics extracted for a reaction order of 1 (refer to [29] for the method utilized). The condensed phase properties considered to be representative are indicated below.

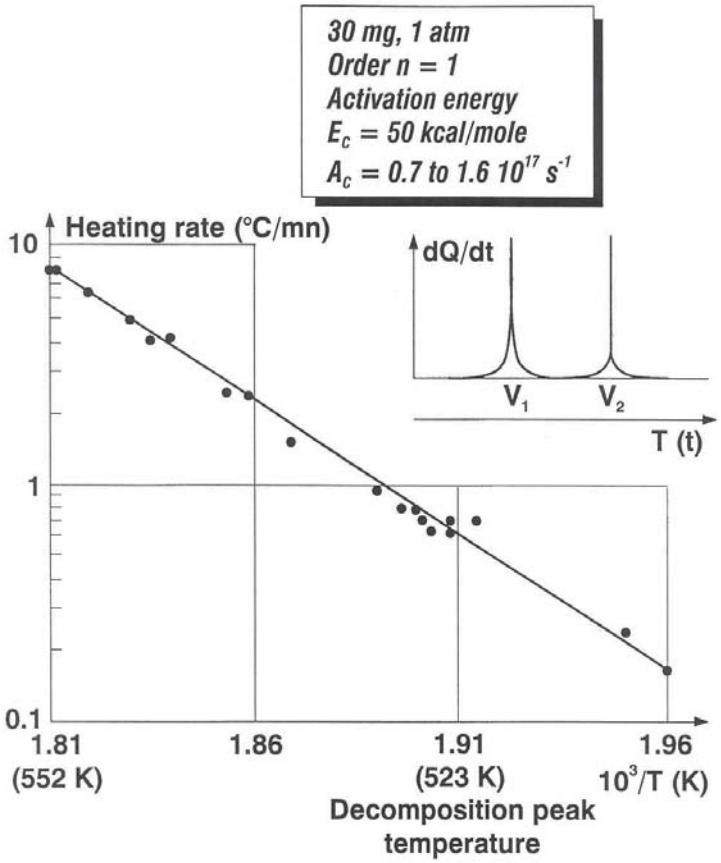


**Figure 22: Differential Thermal Analysis of HMX Decomposition.**

**Table 10: Condensed Phase Properties (Average in the Thermal Wave) for HMX [31]**

| |
|---|
| $\rho_p = 1.9$ g/cm$^3$, $c_p = 0.33$ cal/g K |
| $d_p / \lambda_p / \rho_p c_p = 1\ 10^{-3}$ cm$^2$/s<br>(also found from thermocouple traverses) |
| $\lambda_p = 6.3\ 10^{-4}$ cal/cm s K |

Another technique to obtain the decomposition kinetics, at somewhat higher temperatures, is through ignition tests, by exposing the sample to a given surface heat flux and detecting the delay for the first exothermic ignition reaction (rapid deviation of the surface temperature from that of an inert material). The results are seen on Fig. 23 and confirm those obtained by DTA (the first method gives a good estimate of the activation energy, whereas the ignition experiments are better for estimating the prefactor). All these results correspond to an irreversible thermal decomposition of the HMX bonds with no influence of the pressure.

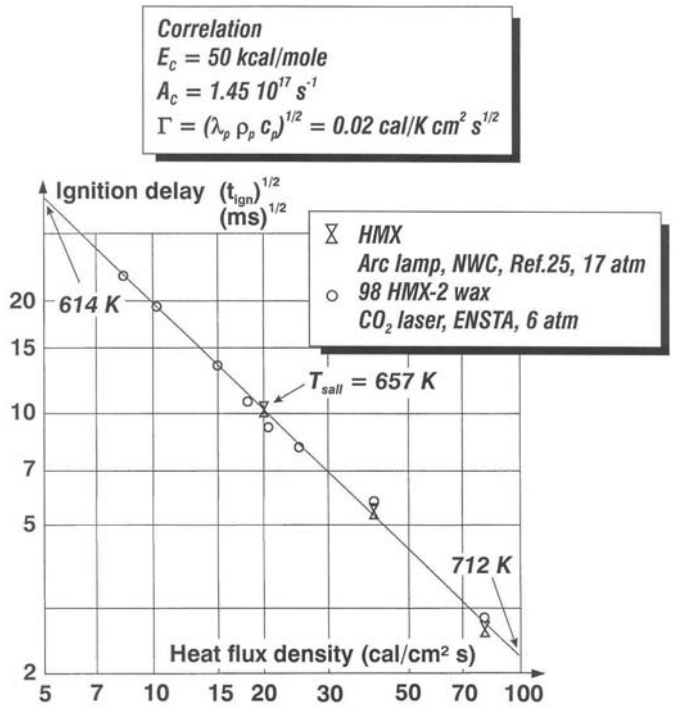


**Figure 23: Ignition of HMX.**

Finally, the investigation of the condensed phase processes under combustion is carried out by determining the temperature profile through the combustion wave by use of micro-thermocouples. As was seen on several occasions the thermal wave thickness is:

$$e_{cond.} = \ln 10^2\ d_p / v_b \qquad (1)$$

that is, in the case of Fig. 24, $e_{cond.} \approx 220$ µm. The thermocouple junction has to be very small, in the present case 5 µm platinum wires are welded end to end by electric discharge with the junction at about this size. A measurement of the thermal diffusivity is also obtained, close to that indicated in Table 10.

The relationship between the surface temperature (obtained from measurements such as that of Fig. 24) and the burning rate is displayed on Fig. 25. Scatter of the measurements is hard to avoid (about 50 K). Also indicated are thermocouple results from reference [28]. The pyrolysis law is also established from the decomposition kinetics obtained by DTA and by ignition experiments, making use of the approach mentioned for double-base propellants as well as for inert binders, according to which [8], for a first order reaction,

$$v_b^2 = ( d_p / \xi_c ) A_c \exp( - \xi_c ) / [( - \ln Y_{p,s} ) ( 1 - T_0 / T_s - Q_s / c_p T_s ) + Q_s / c_p T_s ] \quad (2)$$

$\xi_c \equiv E_c / R T_s$ and $Q_s$ is the heat evolved in the superficial reaction layer of the HMX; its value will be seen next. The amount of HMX at the surface $Y_{p,s}$ is set at 0.01. It is seen that there is continuity between the decomposition (thermal breaking of the chemical bonds, with probably no participation of the vaporization of the HMX) under DTA conditions, ≈ 550 K, for ignition, from 600 to 700 K, and under combustion, up to 900 K. This conclusion on such a continuity, which is not a priori guaranteed, was also reached for double-base propellants (as well as for various binders).

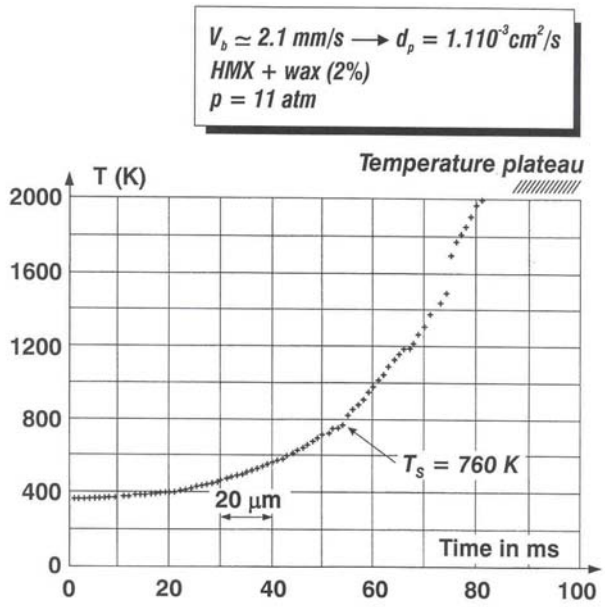


**Figure 24: Temperature Profile, Under Combustion, in HMX by Thermocouple.**

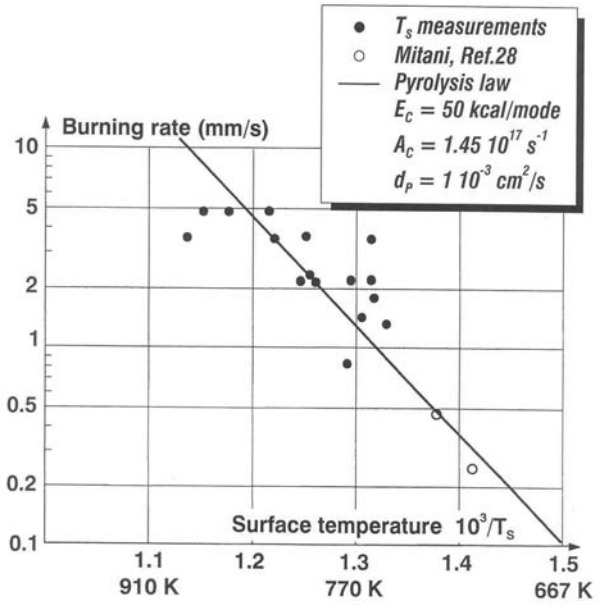


**Figure 25: Pyrolysis Law for HMX.**

From the temperature profiles, as on Fig. 24, the heat evolved in the condensed phase can be evaluated by use of the relation:

$$\lambda_g \, dT / dx|_s = \rho_p v_b [ c_g T_s - c_p T_o - Q_s ] \quad (3)$$

with $Q_s > 0$ if exothermic. The results of Fig. 26 show that indeed the transformation of HMX into gases is exothermic. The energy absorbed by the breaking of the HMX bonds is more than compensated by exothermic reactions taking place in the superficial degradation layer, probably between $NO_2$ and HCHO (see further for the identification of these gases). This mechanism was already observed for double-base propellants.

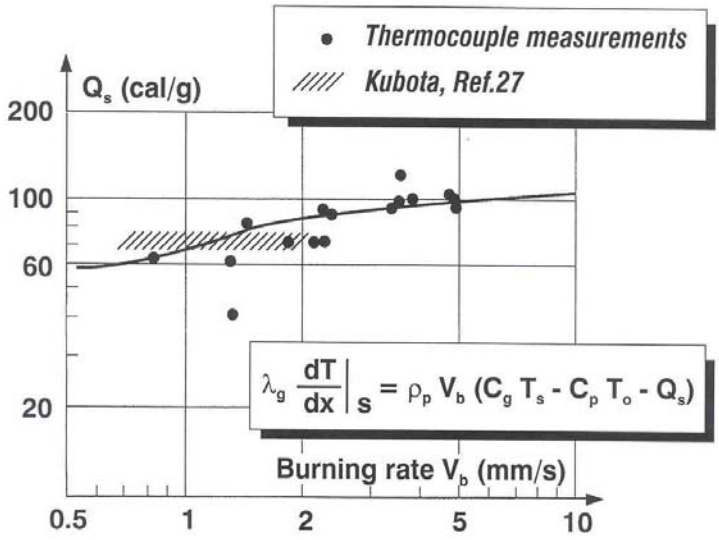


**Figure 26: Heat Evolved in the Condensed Phase of HMX.**

Experiments have been performed [7] by maintaining the linear regression (at about 1 mm/s) of HMX samples with an external heat flux (radiation or contact with a heated plate), under vacuum so as to avoid any gas flame. The sampled gases are then analyzed by mass spectrometry. The following table indicates the results.

**Table 11: Gases Evolved from the Surface of HMX (Mass Fractions [7])**

| $NO_2$ | NO | $N_2O$ | $N_2$ | $CO_2$ | CO | $H_2O$ | $H_2$ | HCHO | HCN |
|---|---|---|---|---|---|---|---|---|---|
| 22.2 | 17.5 | 19.1 | 3 | 1.4 | 1.6 | 3.7 | 0.1 | 14.1 | 16.8 |
| ≈ 59 % | | | ≈ 10 % | | | | ≈ 31 % | | |

It is seen that the initial degradation produces probably $NO_2$ and $N_2O$ in similar amounts and HCHO and HCN. See also for such conclusions reference [32]. Exothermic reactions involving $NO_2$ occur in the superficial degradation layer to give a large amount of NO. Results in rough agreement with those of the above table have also been obtained in Ref. [33] with an infra-red analysis technique.

## 2.0 Gas Phase Behavior

The production from the condensed phase of HMX of several oxidizing gases, $NO_2$, $N_2O$ and NO, can create a two-stage flame. This was seen to be the case for double-base propellants for which $NO_2$ and NO are created in the condensed phase: the primary flame involves $NO_2$ and the secondary flame NO; above ≈ 200 atm the two flames merge into one. In the case of HMX, observation at pressures around 1 atm reveals the existence of a dark induction zone and a detached luminous flame, similar to those of double-base propellants. Also the micro-thermocouple traverses below about 10 atm, such as in Fig. 24, show a plateau in the temperature profile at about 2000 K, much below the final temperature of 3280 K.

The burning rate of HMX, as single crystals or as pressed samples, obtained in Ref. [25] is shown on Fig. 27. The evolution of this burning rate with pressure shows that around 20 atm a pressure exponent of

about 1 is attained, revealing that the staged flame has collapsed into one (as in the case of double-base propellants above about 200 atm).

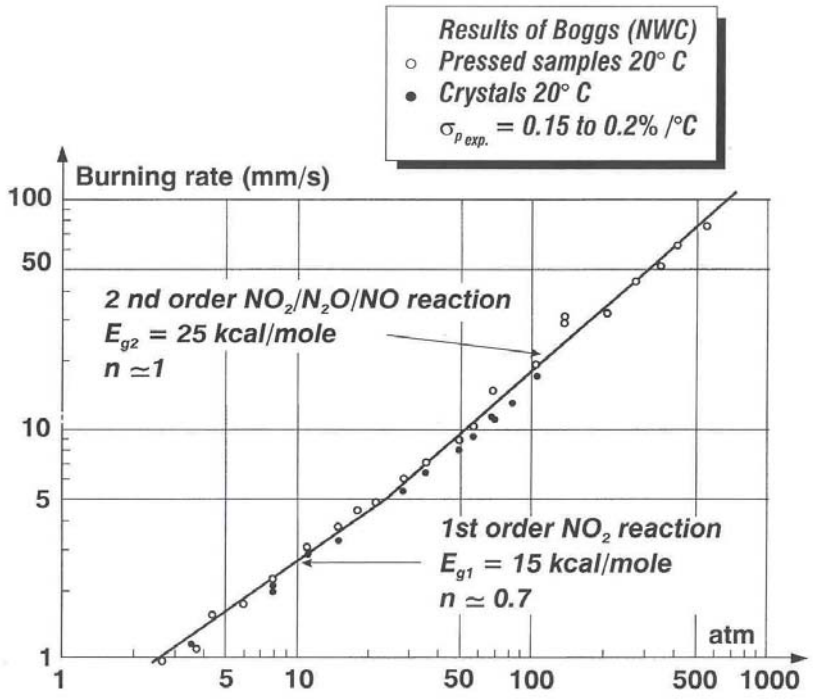


**Figure 27: Burning Rate of HMX.**

It was seen in the chapter on double-base propellants that in the case of a distributed flame an approximation for the temperature profile is:

$$( T_f - T ) / ( T_f - T_s ) = \exp( - 3 x / x_f ) , \quad x_f = 3 \lambda_{g,s} ( T_f - T_s ) / m Q_c , \quad Q_c = c_g T_s - c_p T_0 - Q_s \qquad (4)$$

(at $v_b$ = 10 mm/s this will give $x_f$ = 48 μm, the height to reach $T_f$ within 5 %) and the burning rate becomes:

$$m = \rho_p v_b = [ 3 \langle \omega_g \rangle \lambda_{g,s} ( T_f - T_s ) / Q_c ]^{1/2} \qquad (5)$$

With $\langle \omega_g \rangle$ the summed reaction rate through the flame zone. More complete descriptions of the flame zone can be found in references [29,30], the conclusions of which are essentially those which can be extracted from the above simplified approach.

**Table 12: Values Considered to be Representative of the Gas Phase of HMX**

| |
|---|
| $c_g$ = 0.35 cal/g K, $\lambda_g = 1.25\ 10^{-4} ( T / 700 )^{0.7}$ cal/cm s K |

At low pressures the primary flame, involving $NO_2$ in a first order reaction, controls the burning rate, with, according to Eq. (5), a pressure exponent around 0.5. At higher pressures the collapsed flame is probably dominated by a second order reaction involving NO and $N_2O$, with a pressure exponent close to 1.

## COMBUSTION OF RDX

RDX has a structure similar to that of HMX. The present authors have not considered this component very much, as opposed to HMX. The information comes mostly from the work of Ref. [34].

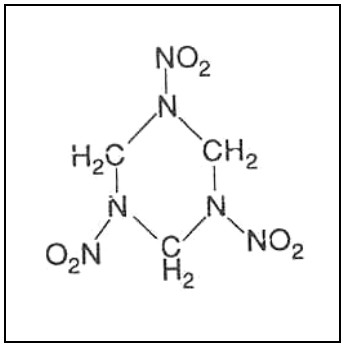


**Figure 28: Chemical Structure of RDX.**

It has been seen that HMX has a behavior somewhat similar to that of a DB propellant, due to the fact that it creates gases which can produce primary and secondary flames, see Table 11. In this case, a very simplified model, based on overall kinetics, shows that the secondary flame dominates the burning rate as soon as 20 to 30 atm (for DB propellants this occurs above 100 atm), in such a way that there is no possibility of creating a super-rate effect (and the accompanying plateau). A much more elaborate model, see Fig. 30, has been presented by Yang et al [34] for RDX. This model takes into account the two condensed phase decomposition paths suggested by Brill, but also incorporates a large amount of evaporation of the RDX (it has to be noted that in the case of HMX, referring to Figs. 22 to 25, the conclusion is reached that the condensed phase process under combustion corresponds to complete decomposition, as observed under DSC-DTA conditions, and thus with no contribution of evaporation). In the melt layer of the RDX (melting temperature supposed at about 470 K) the products of the first decomposition start reacting, much as was seen for double base propellants and for HMX, this being manifested by the gas composition obtained at the surface, see Fig. 30. At the surface, with a temperature depicted on Fig. 29, an important void fraction is computed, corresponding to the amount of RDX which has decomposed in the condensed phase.

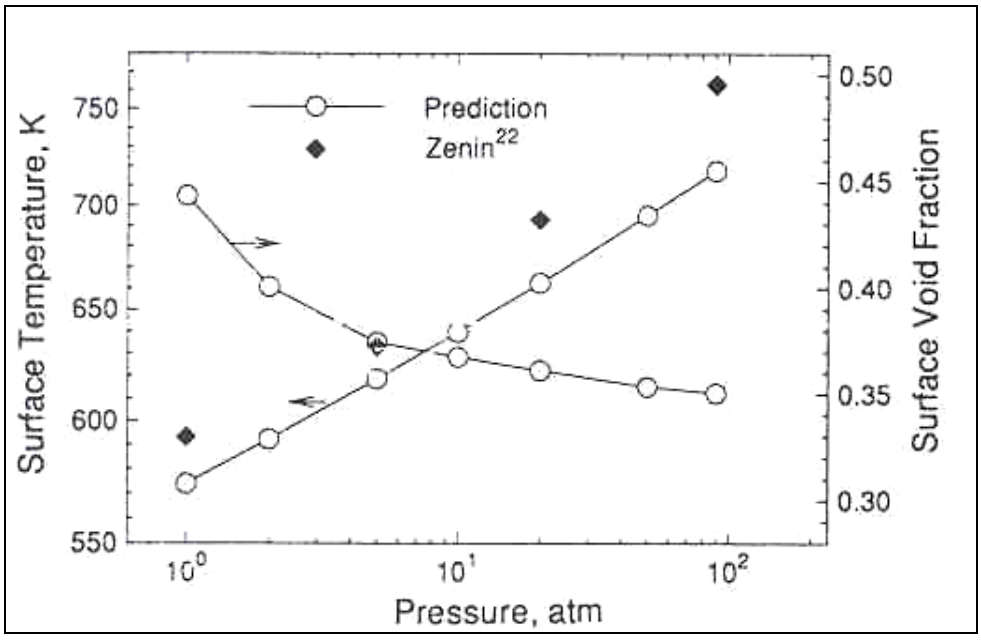


**Figure 29: Conditions at the Surface of RDX [34].**

From T. Brill

$$RDX_{(c)} \xrightarrow{k_1} 3CH_2O + 3N_2O \qquad (R1)$$

$$RDX_{(c)} \xrightarrow{k_2} 3HCN + \tfrac{3}{2}NO + \tfrac{3}{2}NO_2 + \tfrac{3}{2}H_2O \qquad (R2)$$

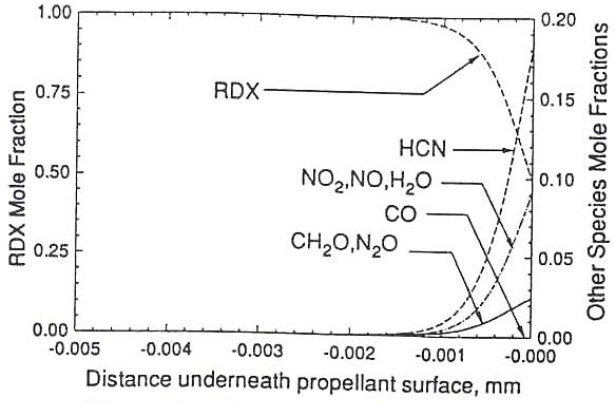


Close-up view of temperature and species-concentration profiles in subsurface region at 90 atm.

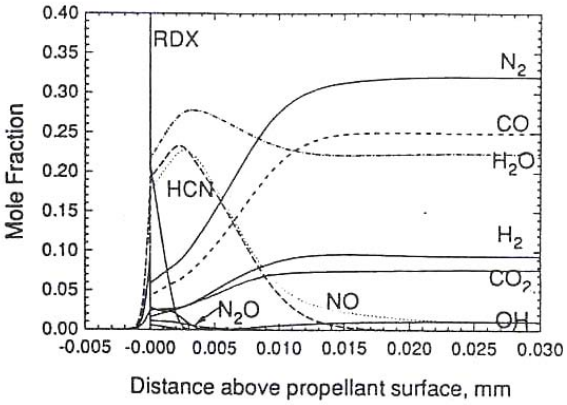


Distributions of temperature and major species concentrations of self-sustained RDX combustion at 90 atm.

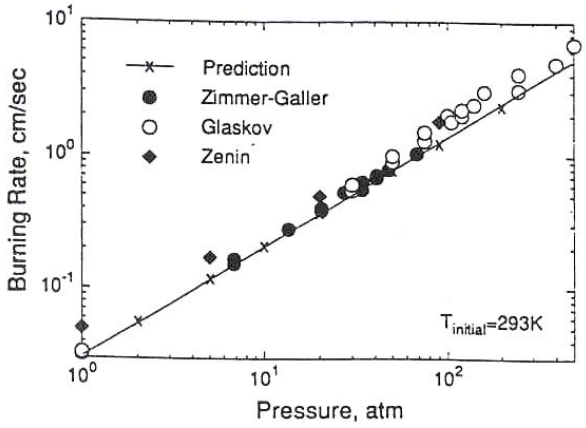


Effect of pressure on strand burning rate of RDX monopropellant.

**Figure 30: Modeling of RDX Combustion [34].**

## COMBUSTION OF CL20 (HNIW)

A new caged nitramine called either CL20 or HNIW (hexaaza hexanitro isowurtzitane) has appeared in the last few years (1987). Because of its high energy content it is envisioned that when combined to an energetic binder, as compared to HMX or RDX compositions, it will be better performing in terms of impulsion and level of burning rate, with smokeless properties maintained and similar safety behavior, Ref. [35].

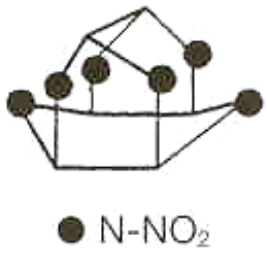


**Figure 31: Chemical Structure of HNIW.**

Differential scanning calorimetry (DSC) and thermogravimetry (TG) contribute to the thermal knowledge of the components to get specific heat, degradation steps and kinetic constants of the material. Helium pycnometry and a thermal diffusivity set-up, at ambient temperature and atmospheric pressure, give the other physical properties. Table 13 brings together the results obtained by these methods. See Ref. [36] for full details.

**Table 13: Thermal and Physical Properties of HNIW**

| Properties | Symbols | SI units | HNIW |
|---|---|---|---|
| Specific heat | $c_p$ | $[J.kg^{-1}K^{-1}]$ | 1004 (± 13 %) |
| Specific mass (density) | ρ | $[kg.m^{-3}]$ | 1980 (± 1 %) |
| Thermal diffusivity | $d_{th}$ | $[m^2.s^{-1}]$ | $0.457*10^{-7}$ (± 6 %) |
| Thermal conductivity | $\lambda=\rho*c_p*d_{th}$ | $[J.m^{-1}K^{-1}s^{-1}]$ | 0.068 |
| Activation energy | $E_A$ | $[J.mole^{-1}]$ | 224000 (± 4.5 %) |
| Frequency factor | $k_0$ or A | $[s^{-1}]$ | If n*=1 $\Rightarrow$ $5*10^{+19}$ |

*n is the reaction order.

The gases evolved from the condensed phase are obtained, as was done for the double base propellants and HMX, with the linear pyrolysis technique under vacuum so as to avoid the gas flame, the regression rate is about 0.5 mm/s.

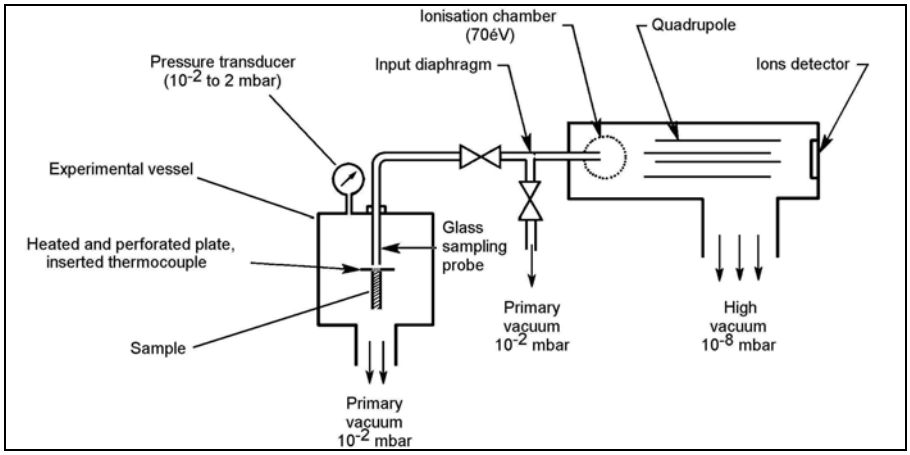


**Figure 32: Set-Up for the Linear Pyrolysis.**

Table 14 shows the results. $NO_2$ and NO are present in large amount, as for HMX, $N_2O$ is in much smaller amount. This gas composition should lead in principle to a staged flame, but due to the high temperature reached at the end of the primary flame, which involves a high mass fraction of $NO_2$, it is likely that the two flames will collapse into one even faster than for HMX.

**Table 14: Molar and Mass Fractions of the Products from HNIW Linear Pyrolysis**

| Species | $NO_2$ | $CO_2$ | $N_2O$ | HNCO | HCHO | NO | HCN | $H_2O$ | CO | $N_2$ | Solid residue 1 | Solid residue 2 |
|---|---|---|---|---|---|---|---|---|---|---|---|---|
| Molar fraction | 0.61 | 0.017 | 0.024 | 0.010 | 0.017 | 0.142 | 0.046 | 0.049 | 0.044 | 0.029 | | |
| Mass fraction | 0.71 | 0.018 | 0.027 | 0.011 | 0.013 | 0.107 | 0.031 | 0.022 | 0.031 | 0.020 | | |
| Mass fraction Gas +Res. | 0.59 | 0.015 | 0.023 | 0.009 | 0.0109 | 0.0899 | 0.026 | 0.0185 | 0.0259 | 0.017 | 0.11 | 0.05 |

Figure 33 gives burning rate measurements for HNIW, on a "strand burner", but it has been now given up in favor of a closed autopressurizable bomb with an ultrasonic measurement technique. This has the advantage of giving the evolution of the burning rate versus pressure with a very low number of experiments, by excursion of a pressure shift during the experiment. Results on ADN, ammonium dinitramide, $NH_4$-N-$(NO_2)_2$, another new oxidizer of interest, is also indicated. These results are in good agreement with most of the literature.

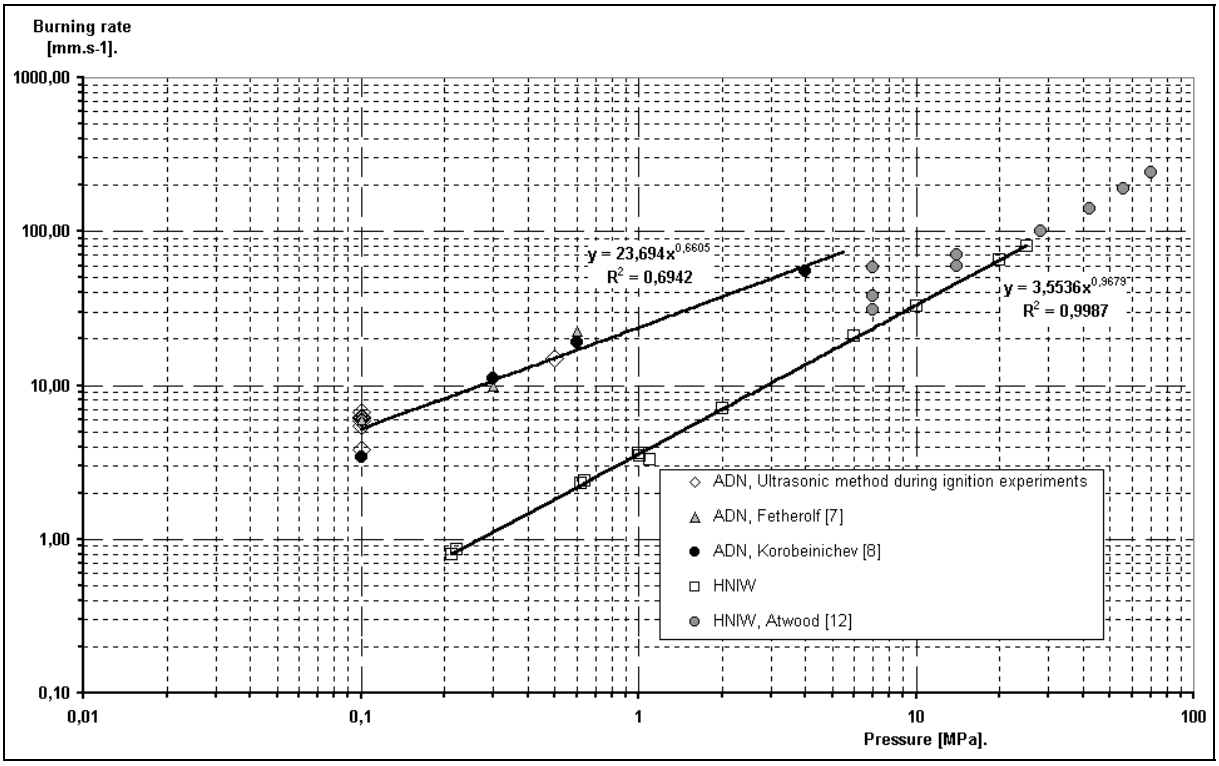


**Figure 33: Burning Rate of HNIW (and ADN).**

Small thermocouples imbedded in the burning sample allow to measure the temperature profile, Fig. 34, the surface temperature, in the vicinity of 800 K, Fig. 36, and from the heat balance at the surface an evaluation of the heat evolved in the condensed phase is obtained, Fig. 35, it is exothermic around 400 kJ / kg, about 100 cal/g similar to the value observed for HMX.

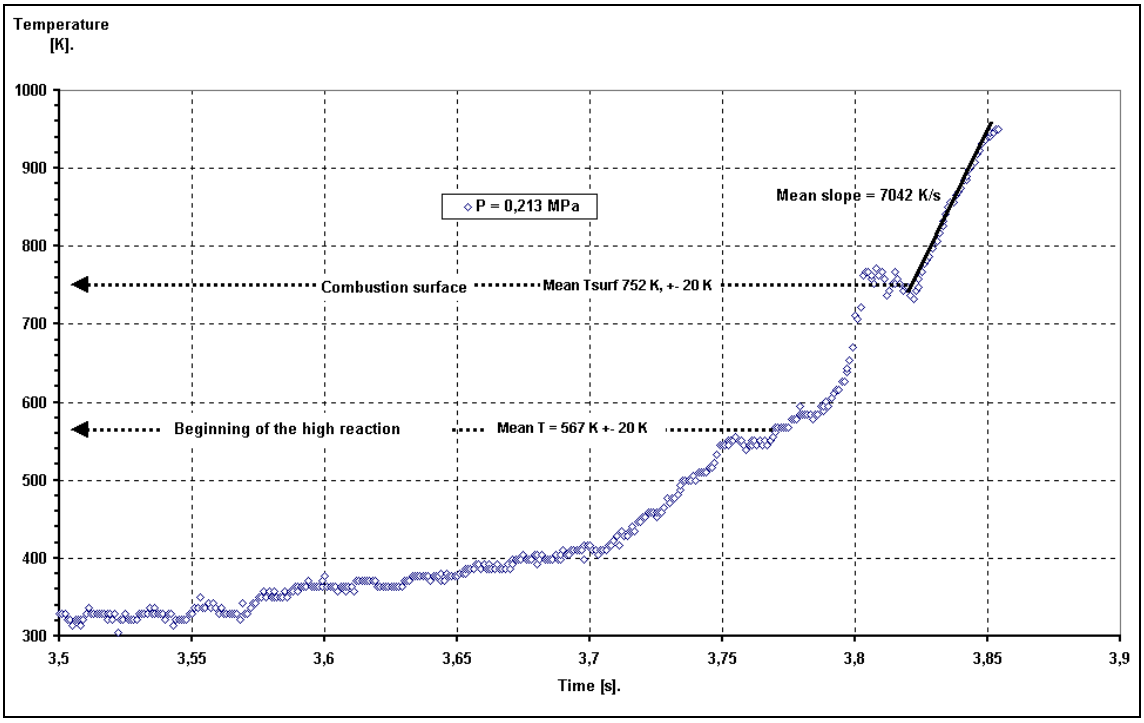


**Figure 34: Temperature Profile in Burning HNIW.**

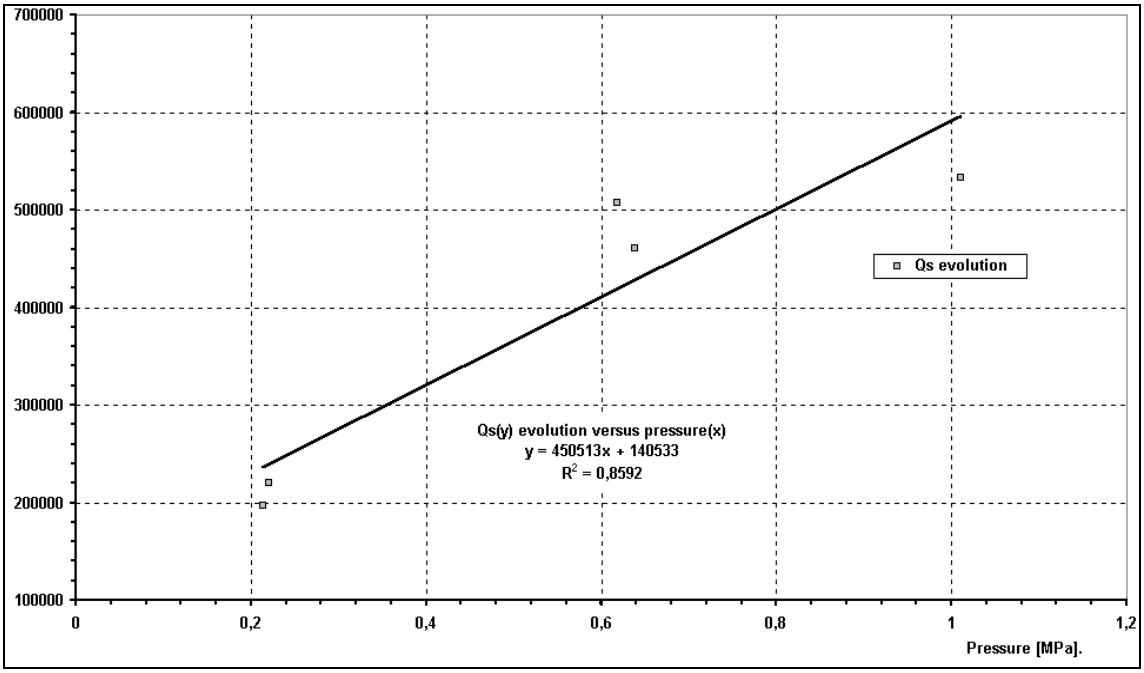


**Figure 35: Energy Released in the Condensed Phase of HNIW, J / kg.**

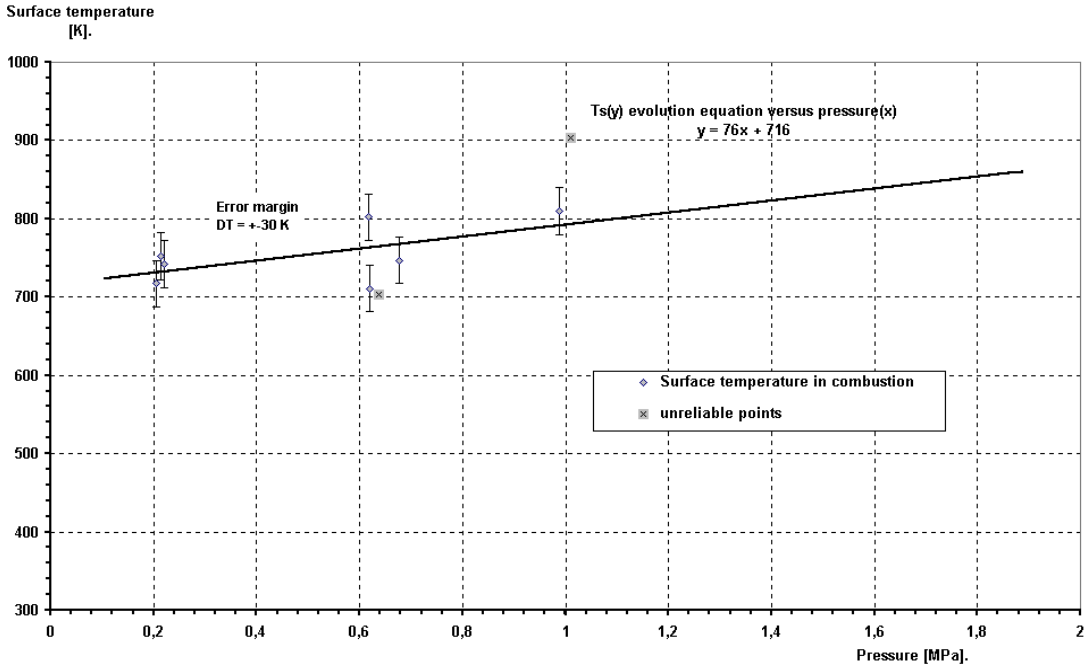


**Figure 36: Surface Temperature of HNIW.**

Figure 37 compares measured surface temperatures and the correlation obtained from the extrapolation (according to the method exposed for HMX) of the condensed phase decomposition kinetics. Taking into account a large uncertainty related to the size of the thermocouple, the agreement is appropriate and found to mean that the decomposition of the HNIW into gases is a purely thermal phenomenon, as measured by DSC, not affected by pressure and with no evaporation entering in the process.

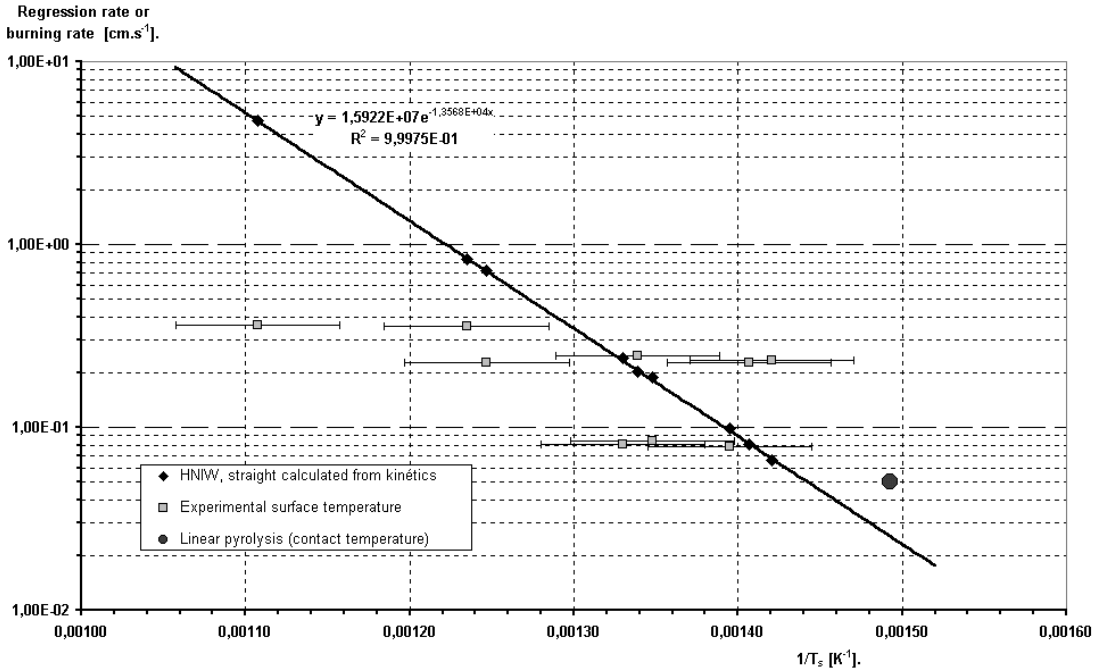


**Figure 37: Surface Temperature vs Regression Rate Correlation.**

# COMBUSTION OF COMPOSITE PROPELLANTS

This chapter is devoted to the description of propellants made of an oxidizer, ammonium perchlorate or HMX, RDX, HNIW, and a binder, inert such as polybutadiene or active, a mixture of a liquid nitrate and a polymer. For the sake of clarity only these two categories will be considered, the main point being, as was said in the introduction, to attempt to improve the understanding of the combustion of propellants rather than to present an extensive catalog of results.

## 1.0 Comparative Picture of Composite Propellants Combustion

Drawing from the results presented previously for the various components, the comparative picture of AP-inert binder and HMX or another nitramine -active binder is found on Fig. 38.

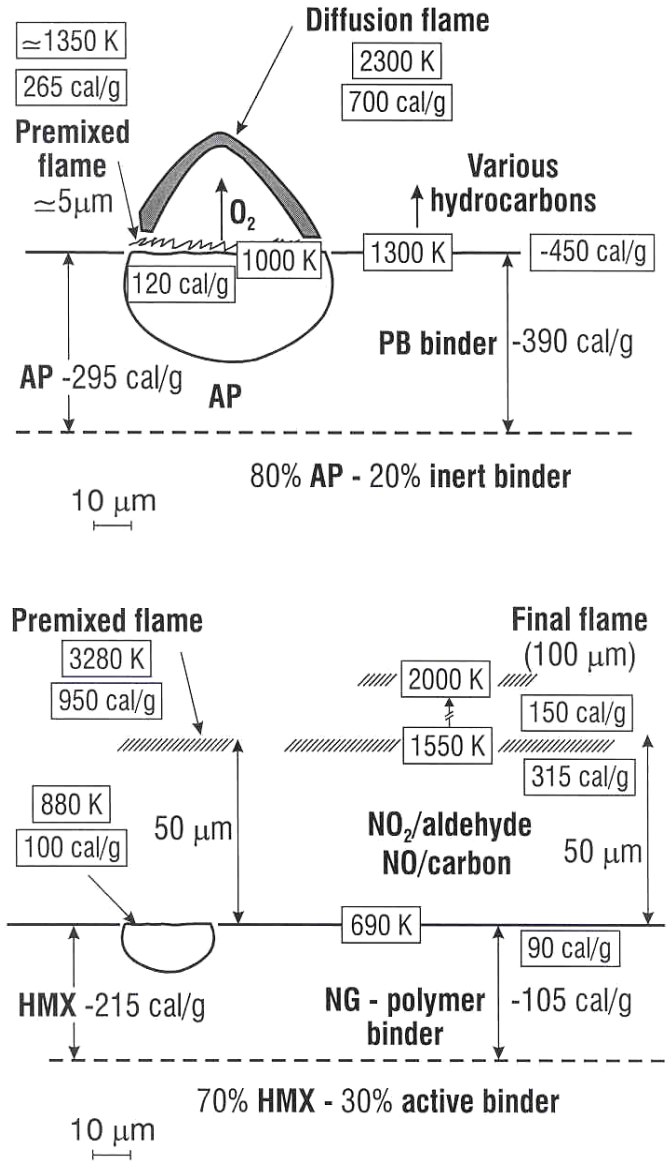


**Figure 38: Comparative Picture of AP-Inert Binder and HMX-Active Binder.**

The *combustion of AP* results in a premixed flame at about 5 μm from the surface at ≈ 1300 K or higher. From this flame 1 mole of $O_2$ comes out for each initial AP mole. From the binder surface at nearly the same temperature, combustible gases are ejected, which, after diffusion, react with $O_2$. As will be seen further on, the diffusion flame height is directly related to the AP particle size. The smaller the particle size the closer is the flame and the higher the heat flux to the surface and therefore the burning rate of the propellant. The pyrolysis of the inert binder is purely endothermic (heat required to bring the temperature to 1300 K and heat to decompose it into gases). In the case of particles of a few tens of μm, the burning of the AP being close to adiabatic (its flame receives some heat flux from the final flame, but computation results show that there is only a moderate deviation from adiabatic conditions), the heat flux from the final flame serves primarily to keep the binder regressing.

*The combustion of HMX or another nitramine* is also through a premixed flame, about 50 μm from the surface, reaching the final stage of 3280 K (for HMX). The gases emitted from this flame cannot sustain any further combustion. The active binder goes through its own combustion, with a primary flame reaching ≈ 1550 K some 50 μm from the surface. The final flame somewhat further away reaches about 2000K. There is no direct interaction between the two components of the propellant. The burning of the propellant is then an average of the individual burning rates. There exist however an indirect interaction of the active binder on the HMX particles. As was seen, the thermal properties of HMX and the active binder are close and the HMX particles are immersed in the temperature profile of the binder. Upon reaching the surface the top of the particle is at about 700 K, the surface temperature of the binder. This so happens to be very much the temperature for first ignition of HMX (see Fig. 23). There will be however a transition delay of the HMX particle to full combustion for which its surface temperature is about 900 K. This will be dealt with in more details further on.

In the case of AP, the ignition temperature is around 650 K and the surface temperature for full combustion is around 900 to 1000 K. Immersed in the inert binder with a surface temperature of ≈ 1300 K, the AP should reach combustion as soon as it is uncovered with no transition delay.

## 2.0 Propellant Burning Rate Resulting from Component Rates

Various approaches have been presented in the literature to build the propellant burning rate from the components' own burning rates. One of the first comprehensive models for composite propellant combustion modeling, Ref. [37], had a picture of AP and binder burning in parallel with a partitioning of the surface between the two ingredients and a surface averaged propellant burning rate. This view is also found in Refs. [38,39], with Ref. [40] being a complete review for AP-inert binder propellants, including references preceding the work of [37]. A view of a sequential burning mechanism, in which a given path goes through oxidizer particles separated by layers of binder, Fig. 39, with as a consequence a time averaged propellant burning rate, was first presented in Ref. [42].

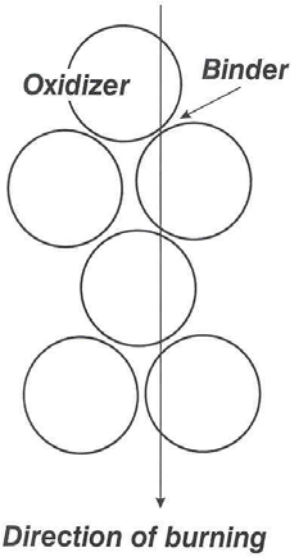


**Figure 39: Time Averaged Propellant Combustion.**

This viewpoint is subscribed to in the present work, as was done in Ref. [43], although the details have since then evolved into the option presented herein (which seems to be coherent with the latest view of

M. Beckstead [45]. Averaging of the components' burning rates, HMX and active binder, in Ref. [41] into the propellant burning rate is obtained by assuming that the components melt and mix at the surface and then form an average premixed gas flame. Due to the very small thickness of the melt (to the extent that melting occurs) layers (of the order of μm) and very short residence times in these layers (tenths of ms), it is believed that such premixing of the components should not take place. This is also the conclusion of [45].

Finally, in the recent work of Ref. [44], a surface average is operated for AP-binder interactions whereas a time average HMX-binder approach is adopted within the same mixed oxidizers propellant.

*In a randomly packed arrangement of oxidizer spheres* of diameter $D_{ox}$, with the average height through the sphere from a given direction (perpendicular to the surface) $h_{ox}$, and for a volume of 1 $cm^2$ on the surface by 1 cm in depth, the number of particles intercepted along 1 cm of length being N, one has:

$$N h_{ox}\ 1\ cm^2 / N h_b\ 1\ cm^2 = \xi_{ox} / ( 1 - \xi_{ox} ) \quad (1)$$

with $h_b$ the average binder height between particles and $\xi_{ox}$ the volume fraction loading in oxidizer. Then it comes:

$$h_b = h_{ox} ( 1 - \xi_{ox} ) / \xi_{ox} \quad (2)$$

and due to

$$N ( h_{ox} + h_b ) = 1\ cm,\ N = \xi_{ox} / h_{ox} \quad (3)$$

For a propellant burning rate $v_{b,p}$, the time to run through 1 cm of depth is

$$t = 1 / v_{b,p} = t_{ox} + t_b = N h_{ox} / v_{b,ox} + N \Delta t_{ox} + N h_b / v_{b,b} \quad (4)$$

$\Delta t_{ox}$ being the (possible) transition delay to full combustion after the top of the oxidizer particle has reached the surface. Then the propellant burning rate, as expressed with the component burning rates, is, with Eq. (3) taken into account,

$$1 / v_{b,p} = \xi_{ox} / v_{b,ox} + \xi_{ox} \Delta t_{ox} / h_{ox} + ( 1 - \xi_{ox} ) / v_{b,b} \quad (5)$$

Consideration of a sphere being traversed randomly along a given direction leads after some computation to $h_{ox} = D_{ox} ( \pi / 4 )^2$.

In the *case of AP- inert binder propellants with no transition delay*, the propellant burning rate is

$$1 / v_{b,p} = \xi_{ox} / v_{b,AP} + ( 1 - \xi_{ox} ) / v_{b,b} \quad (6)$$

The relation ship between volume fraction loading ξ and mass fraction loading α being

$$\alpha_i = \xi_i \rho_i / \rho_p \quad (7)$$

$$\sum \xi_i = 1\ ,\ 1 / \rho_p = \alpha_{ox} / \rho_{AP} + ( 1 - \alpha_{ox} ) / \rho_b \quad (8)$$

that is for example for an 88 % AP - 12 % PB binder $\rho_p = 1.72\ g/cm^3$.

The mass burning rate of the propellant is

$$m_p = \rho_p v_{b,p}$$

and Eq. (6) yields

$$1 / m_p = \alpha_{ox} / m_{AP} + ( 1 - \alpha_{ox} ) / m_b \quad (9)$$

In the *case of a propellant loaded with aluminum*, it is known that the aluminum particles are ejected from the surface [46,47] (Ref. [47] being an extensive review of the processes of aluminum combustion) and burn at several hundreds of µm from the surface. The view of the combustion of aluminum is summarized here, see Figs. 40,41,42.

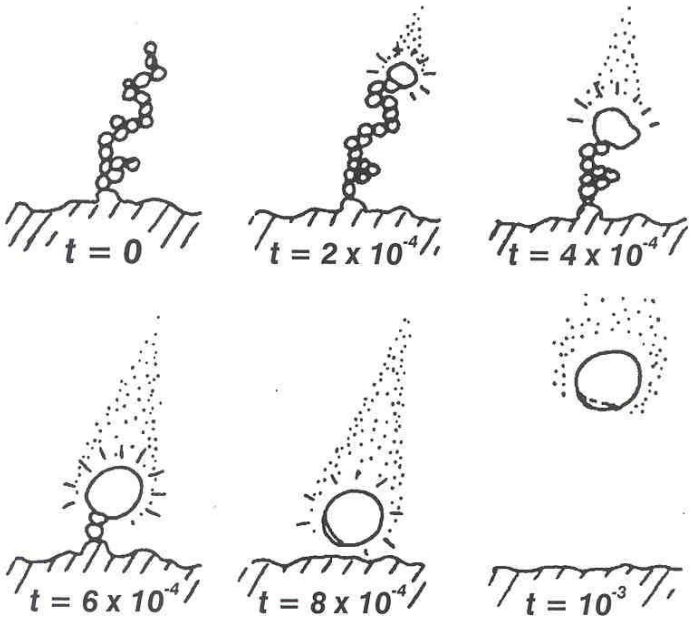


**Figure 40: Visualization of Aluminum Behavior (From Ref. [47]).**

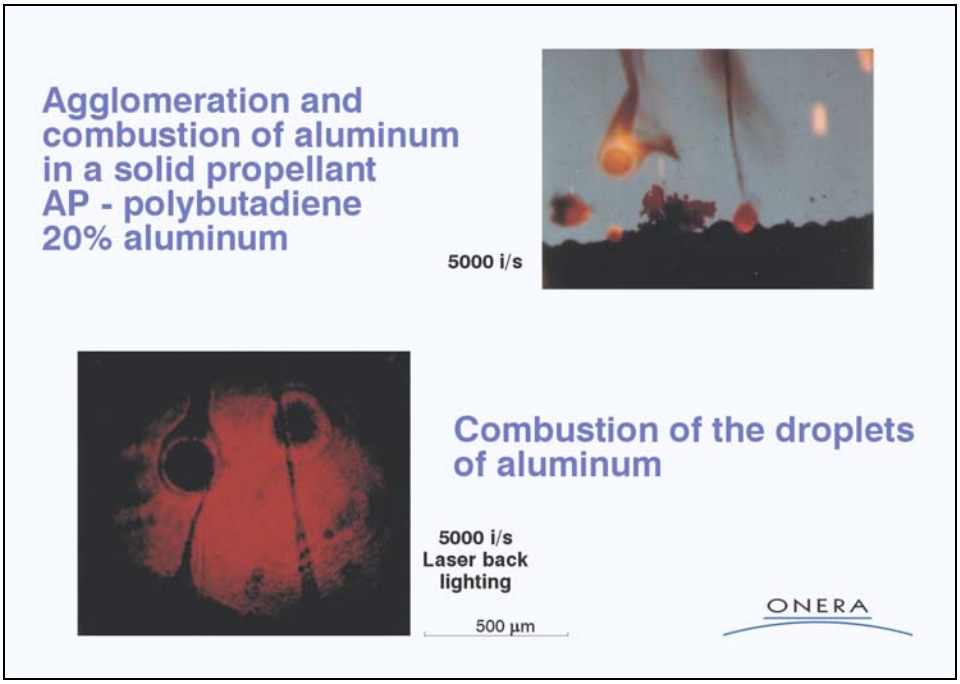


**Figure 41: Aluminum Combustion.**

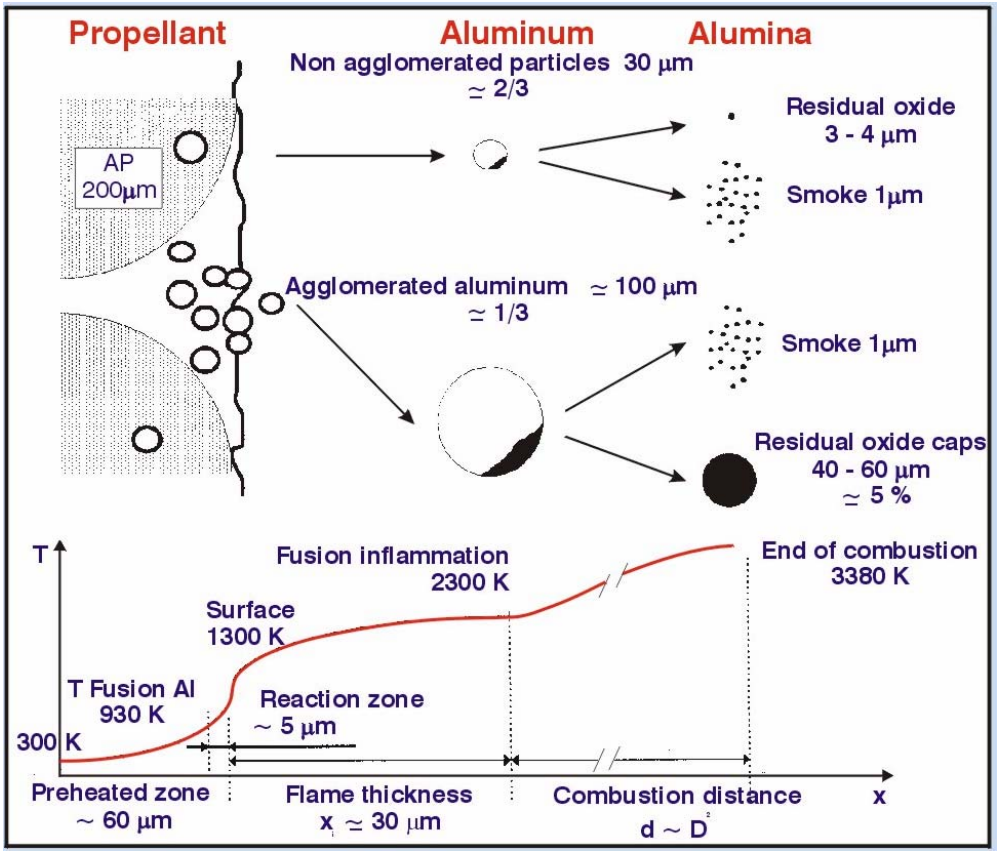


**Figure 42: Behavior of Aluminum (18 %) in a Composite Propellant.**

- Aluminum melts at 930 K (inert binder reaches about 1300 K) (active binder reaches about 700 K) and individual particles aggregate in part into clusters.
- Sketches of selected frames of high speed motion pictures, Fig. 40, illustrate a protracted (because the protective $Al_2O_3$ coating melts at 2300 K) ignition-agglomeration event in which the hottest portion of the accumulate inflames and precipitates the complete inflammation-agglomeration of the (already hot) accumulate.
- The $Al_2O_3$ protective coating collapses into cap, exposing the Al globule (typically ≈ 100 µm).
- Aluminum vaporizes at ≈ 3300 K and reacts in nearly-spherical flame with $CO_2$ and $H_2O$ from AP-binder flame.
- The caps give $Al_2O_3$ particles of a few tens µm, the spherical flames give $Al_2O_3$ smoke of ≈ 1µm.
- Not all aluminum particles go into accumulates (packs of original particles sticking together) from pockets within large AP particles. About 2/3 of the original particles escape individually from the surface, giving as combustion product essentially 1 µm smoke [48].

The volume fractions being

$\xi_{ox}$ , $\xi_b$ , $\xi_{al}$

Eq. (8) becomes

$$1 / \rho_p = \alpha_{ox} / \rho_{ox} + \alpha_b / \rho_b + \alpha_{al} / \rho_{al} \qquad (10)$$

that is, for example, for a 70 % AP, 20 % aluminum ($\rho_{al}$ = 2.7 g/cm$^3$), 10 % PB binder ($\rho_b$ = 0.92/cm$^3$), $\rho_p$ = 1.84 g/cm$^3$.

With respect to the burning rate of the propellant loaded with aluminum it is obtained:

$$1 / v_{b,p} = \xi_{ox} / v_{b,ox} + N_{al}\, h_{al} / v_{b,al} + N_{al}\, \Delta t_{al} + \xi_b / v_{b,b} \qquad (11)$$

The "burning" rate of aluminum can be considered as infinite since it is ejected from the surface, whereas its "transition delay" is the time for the binder to regress through the particle height:

$$\Delta t_{al} = h_{al} / v_{b,b}$$

Also, for each component N h = $\xi$ its volume fraction loading. The propellant burning rate becomes

$$1 / v_{b,p} = \xi_{ox} / v_{b,ox} + \xi_b / v_{b,b} + \xi_{al} / v_{b,b} = \xi_{ox} / v_{b,ox} + ( 1 - \xi_{ox} ) / v_{b,b} \qquad (12)$$

that is the relation which would be obtained for a corresponding propellant with no aluminum, with the binder filling in for it.

From an energetics point of view the modeling of the combustion of aluminized propellants should include at the surface the heat of fusion of aluminum ≈ 95 cal/g of Al. One can see Ref. [49] for such an approach.

## 3.0 HMX (or RDX) (or HNIW) – Active Binder Propellants

Both HMX and the active binder have independent burning rates. The resulting propellant burning rate is given by Eq. (5), where the transition delay has to be evaluated.

The emerging HMX particle offers to the external heat flux the surface area of the sphere cap which has been exposed by the binder regressing at $v_{b,b}$ after the time t from first appearance has evolved:

$$S = \pi\, D_{ox}\, ( v_{b,b}\, t )$$

With $\alpha$ being the part of the sphere which is heated by the superficial flux $\Phi$ , the temperature rise is

$$\alpha\, ( \rho_p\, c_p )_{ox}\, dT / dt\, ( 4\, \pi / 3 )\, ( D_{ox} / 2 )^3 = \Phi\, \pi\, D_{ox}\, v_{b,b}\, t \qquad (13)$$

The heat flux received is that of the binder flame when the particle first emerges and it transitions to that of the HMX flame when the particle has reached full combustion, a transition formula being assumed to be

$$\Phi = \Phi_b + [\, ( T_s(t) - T_{s,b} ) / ( T_{s,ox} - T_{s,b} ) \,]\, ( \Phi_{ox} - \Phi_b )$$

with

$$\Phi_{ox,b} = \rho_p\, v_b\, ( c_g\, T_s - c_p\, T_o - Q_s )|_{ox,b}$$

The fraction of the sphere heated by the flux is taken to be, with K finally adjusted at 0.1,

$$\alpha = \exp( - K\, D_{ox} / e_p^* )$$

$e_p^*$ is the thermal wave thickness for which the temperature is at 90 % of its surface value, that is, sufficiently close to it,

$$( T - T_o )/( T_s - T_o ) = 0.9 = \exp( - e_p^* v_{b,b} / d_p ) \quad (14)$$

When $D_{ox} / e_p^* \rightarrow 0$ the particle is vanishingly small with respect to the thickness of the layer at about the surface temperature, $\alpha \rightarrow 1$ and the particle is heated in its entirety by the heat flux. If $D_{ox} / e_p^* \rightarrow \infty$ the particle is very large compared to the surface layer, $\alpha \rightarrow 0$, it is heated on a vanishingly small part. When $D_{ox} = e_p^*$ , $\alpha = 0{,}9$, the particle is immersed in the binder layer at $T \approx T_{s,b}$ and it is almost totally heated by the external flux. The transition delay from Eq. (13) is then

$$\Delta t_{ox}^2 = \alpha ( \rho_p c_p )_{ox} ( D_{ox}^2 / 3 v_{b,b} ) [ ( T_{s,ox} - T_{s,b} ) ] / ( \Phi_{ox} - \Phi_b )] \ln( \Phi_{ox} / \Phi_b ) \quad (15)$$

One noteworthy feature of this relation is that the transition delay is proportional to the particle size $D_{ox}$, in such a way that inserted in Eq. (5) it renders the burning rate insensitive to $D_{ox}$, a fact which is observed experimentally for HMX-energetic binder propellants [43].

Figures 43 and 44 show two examples of propellant burning rate laws with the corresponding component rates. It is seen that the propellant burning rate is intermediate between those of HMX and of the binder (its being close to that of the binder at pressures under 100 atm is coincidental).

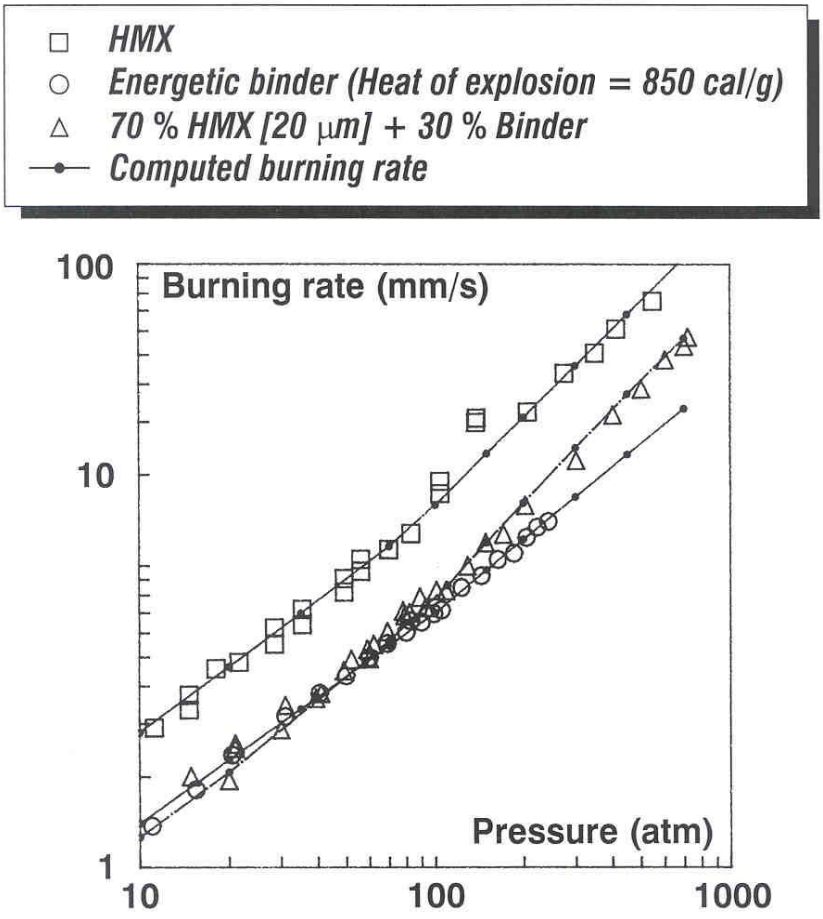


**Figure 43: Experimental and Computed Burning Rate of a Nitramine Based Propellant.**

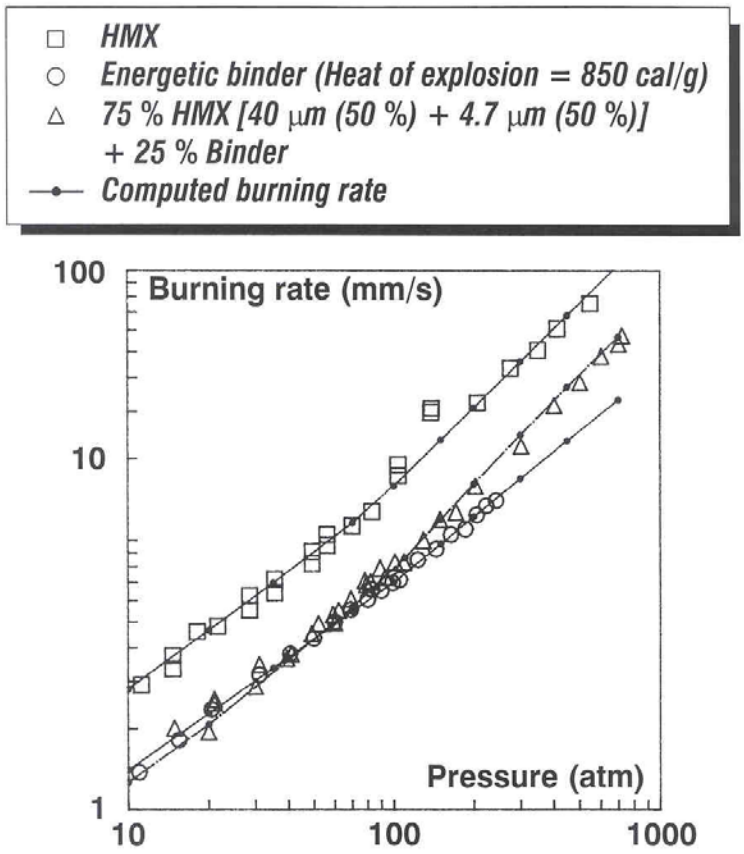


**Figure 44: Experimental and Computed Burning Rate of a Nitramine Based Propellant.**

The model presented above, and, what is important, the mechanisms it takes into account (that is the absence of diffusional interaction between the components and the importance of a transition delay for the HMX particles), is quite representative of the experimental results. Some of the details of the making of the burning rate are given in Table 15.

**Table 15: Elements for the Evaluation of the Burning Rate (70 % HMX – 30 % Active Binder)**

| PRESSURE | 20 atm | 100 atm | 250 atm |
|---|---|---|---|
| $v_{b,b}$ | 2,4 mm/s | 7,1 | 14,5 |
| $T_{s,b}$ | 622K | 667 | 698 |
| $v_{b,ox}$ | 4,5 mm/s | 17 | 37,5 |
| $T_{s,ox}$ | 828K | 907 | 962 |
| % of burning time due to delay | 32 % | 16 % | 4 % |
| $v_{b,p}$ | 2,3 mm/s | 9,4 | 22,7 |

It is seen that at low pressures the transition delay has a strong impact and the burning rate of the propellant happens to fall close to that of the binder. At high pressure the propellant burning rate is nearly the time average of the component rates (without delay the average at 250 atm is 24 mm/s).

It is observed that, for a given HMX-energetic binder composition, the burning rate law is locked and that there is no way to tailor it (as can be done in AP-inert binder compositions by acting upon the particle size). Furthermore the pressure exponent is too high to be acceptable for the motor operation. Attempts to act upon the HMX burning rate by the use of additives have not been successful. One possibility of action however is with additives specific to double-base propellants, lead and copper salts and carbon black, incorporated in the active binder. It has been found on Fig. 12 that a moderate super rate effect can be obtained. It is seen on Fig. 45 that such a modified binder associated with HMX, and after optimization of the amount and of the size of the additives, yields a burning rate law with moderate pressure exponent and initial temperature sensitivity.

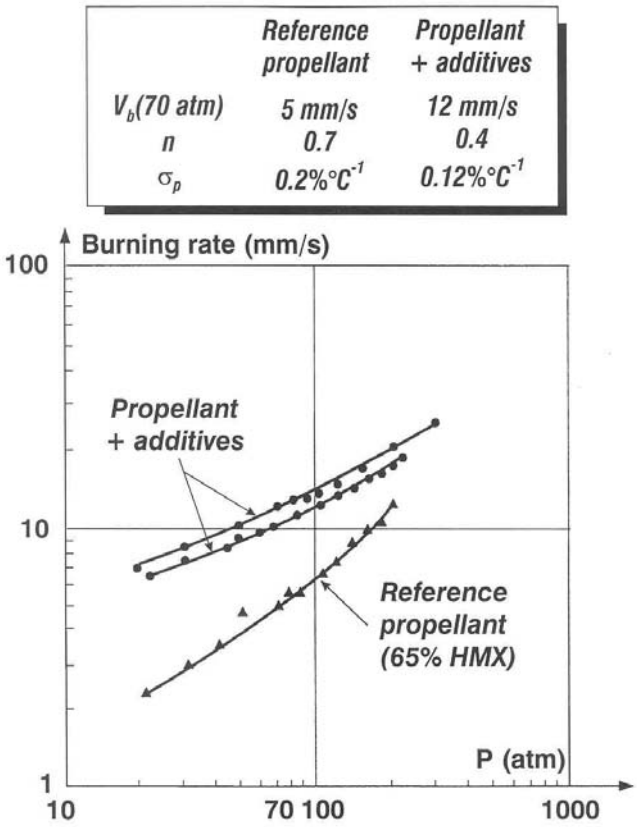


**Figure 45: HMX – Active Binder Propellant with Additives.**

Propellants based on the new oxidizer HNIW and binders made from GAP (glycidyl azide polymer) have been considered. GAP has been studied in Refs. [50,51] with the techniques employed for the double base propellants, in particular its surface temperature under combustion is similar, around 800 K. In the actual binder GAP is associated to a liquid nitrate ester, see Ref. [35], the behavior of which is very close to a cool active binder. The modelization has been applied to these propellants (in particular assuming no interaction, other than the transition delay for the full burning of the oxidizer), it can be seen to give a proper account of the resulting burning rate, Fig. 46. As opposed to HMX or RDX which are balanced to give CO, $H_2O$ and $N_2$, HNIW is over oxygenated to give

$$C_6H_6N_{12}O_{12} \rightarrow 6\ CO + 3\ H_2O + 6\ N_2 + 3 / 2\ O_2$$

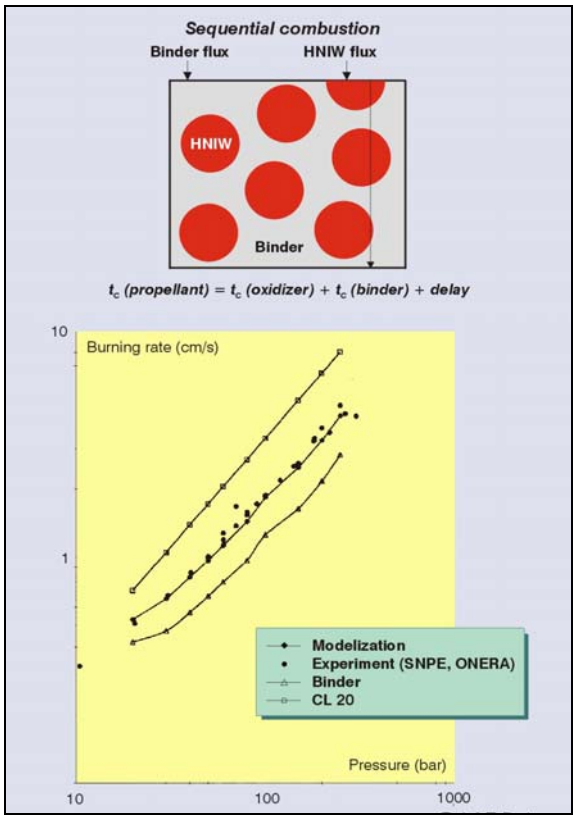


**Figure 46: HNIW (60 %) – Binder GAP + Nitrate Ester.**

A possible recombustion with the gases from the flame of the active binder could be conceivable, this implying an influence of the oxidizer particle size and a possibility of regulating the burning rate as in AP composite propellants. The modelization does not confirm this possibility. Comparing propellants with different particle sizes would clarify this point.

## 4.0 AP-Inert Binder Propellants

The burning rate of a propellant based on AP and an inert binder such as HTPB is thought to be described by the averaging rule of Eq. (9) from the burning rates of the components. In this case the binder has of course no autonomous burning rate. Its regression rate is due to the heat flux from the diffusion flame, as depicted on Fig. 38, between $O_2$ from the AP flame and the hydrocarbons from the pyrolysis of the binder. A description of such a flame is given here.

A column of $O_2$ containing gases is ejected from a particle with an efficient diameter $D_{ox}$* proportional to $D_{ox}$ at a velocity $v_g$, such that $m_p = \rho_g v_g$. This column is consumed by a *lateral diffusion* characterized by a diffusion velocity

$$v_{diff} = A_d \, \text{Đ} \, / \, ( D / 2 ) \qquad (16)$$

D being the local diameter of the column, $A_d$ some constant of order 1 and **Đ** the diffusion coefficient in $cm^2/s$. The variation of the column diameter is then given by

$$dD = - 2 \, v_{diff} \, dt \, , \, dx = v_g \, dt$$

$$D \, dD = - 4 \, A_d \, \text{Đ} \, dx / v_g$$

Resulting in

$$D_{ox}^{*2} = 8\, A_d\, \mathbf{Đ}\, x_{fd} / v_g,\ x_{fd} = D_{ox}^{*2}\, m_p / 8\, A_d\, \rho\, \mathbf{Đ} \qquad (17)$$

In this relation $D_{ox}^{*}$ is the average diameter of a sphere cut randomly by a plane

$$D_{ox}^{*} = 2\, D_{ox} / \sqrt{6}$$

When the lateral diffusion of $O_2$ and hydrocarbon gases into each others is purely laminar the diffusion coefficient is expressed as:

$$\mathbf{Đ} = \mathbf{Đ_0}\, T^{\alpha} / p\ ,\ \rho\, \mathbf{Đ} = \mathbf{Đ_0}\, T^{\alpha - 1}\, M / R$$

(with the equation for perfect gases $p / \rho = R\, T / M$ being used) and the flame stand-off distance

$$x_{fd} = D_{ox}^{*2}\, m_p\, (\, R / M\,) / 8\, A_d\, \mathbf{Đ_0}\, T^{\alpha - 1} \qquad (18)$$

does not depend explicitly upon the pressure. In this limiting case and due to the fact that

$$m_p \sim 1 / x_f\ ,$$

it is obtained

$$m_p \sim 1 / D_{ox}$$

independent of the pressure level and directly dependent on the particle size.

As will be seen later, it has been found that the diffusion flame process might become turbulent at high pressures when large differences exist between the mass flow rates emitted from the AP and from the binder. This conclusion is also mentioned in reference [40]. A general expression for a turbulent transport coefficient is

$$\rho\, \mathbf{Đ} \sim \rho\, u'\, \ell$$

with u' the magnitude of the fluctuating gas velocity and $\ell$ its scale. It is then assumed

$$\ell \sim D_{ox} / 2\ ,\ \rho\, u' \sim (\, m_{ox} - m_b\,)$$

that is the turbulent enhancement is related to the difference between the mass flow rates within the $O_2$ containing column and in the surrounding gases. Then Eq. (17) becomes

$$x_{fd} = D_{ox}^{*2}\, m_p / 8\, A_d\, (\, \rho\, \mathbf{Đ}\,)_{eff} \qquad (19)$$

$$(\, \rho\, \mathbf{Đ}\,)_{eff} = \mathbf{Đ_0}\, T^{\alpha - 1}\, M / R + K\, (\, D_{ox} / 2\,)\, (\, m_{ox} - m_b\,) \qquad (20)$$

where K should be of the order of 0.1.

An extra *flame thickness related to the chemical time* for the completion of the $O_2$-hydrocarbons reaction should be taken into account. It is obtained

$$x_{fr}\ (\sim v_g\ \tau_{ch} \sim m\, \tau_{ch} / \rho \sim m / \omega) = m_p / A_r\, p^2\, A_{g,f}\, \exp\,(\, - E_{g,f} / R\, T_f\,) \qquad (21)$$

the characteristics being related to the final $O_2$ - hydrocarbons flame.

The stages of the combustion of an AP propellant are shown on Fig. 47, which is to be seen side by side with Fig. 38 for the corresponding values. The temperature profiles are approximated as

$$( T_f - T ) / ( T_f - T_s ) = \exp( - 3 x / x_f ) \quad (22)$$

with

$$q_s = 3 \lambda_{g.s} ( T_f - T_s )/ x_f \quad (23)$$

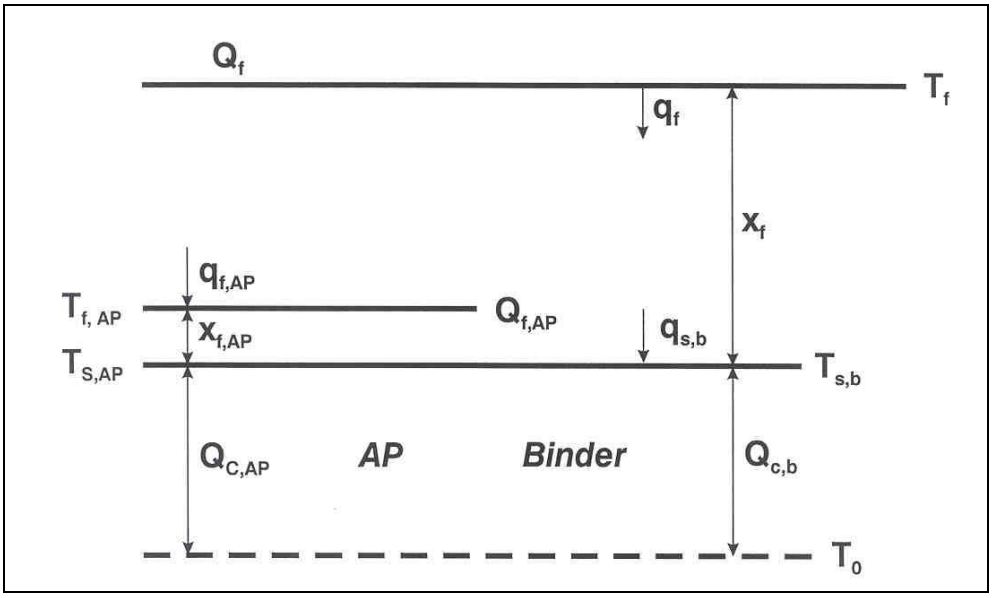


**Figure 47: Stages of an AP – Inert Binder Propellant.**

The *mass regression rate of the binder* is then given by

$$m_b Q_{c,b} = q_{s,b} = 3 \lambda_{gs} ( T_f - T_{s,b} ) / x_f \quad (24)$$

where the constituting elements of this relation have been seen in the chapter on inert binders. It should be noticed that, to simplify the description, a uniform mass flow rate $m_p$ is taken in the gas phase above the binder and the AP flame. The flame height $x_f$ is then the sum of Eqs. (19 and 21).

*The mass burning rate of the AP*, see Eq. (13) of the corresponding chapter,

$$m_{AP} = [ 3 <\omega_{AP}> \lambda_{g,s} ( T_{f,AP} - T_{s,AP} ) / Q_{c,AP} ]^{1/2} \quad (25)$$

$$3 <\omega_{AP}> = p^2 A_{g,AP} \exp[ - E_{g,AP} / R T_{f,AP} ]$$

Now, due to the fact that the AP flame receives a heat flux from the final flame, the flame temperature is no longer the adiabatic temperature ( $T_{f,AP}^{ad} = 1205$ K ). It is given by

$$m_{AP} c_g ( T_{f,AP} - T_{s,AP} ) + m_{AP} Q_{c,AP} = m_{AP} Q_{g,AP} + q_{f,AP} \quad (26)$$

with, from Eq. (22), applied between $x_{f,AP}$ and $x_f$ the heat flux from the main flame into the AP flame

$$q_{f,AP} = 3 \lambda_g ( T_f - T_{f,AP} ) / ( x_f - x_{f,AP} ) \quad (27)$$

Results for the burning rate of AP-HTPB propellants are indicated on Fig. 48, where is seen a strong influence of the AP particle size. The model described above, and what is important the mechanisms it contains, gives a satisfactory account of these results.

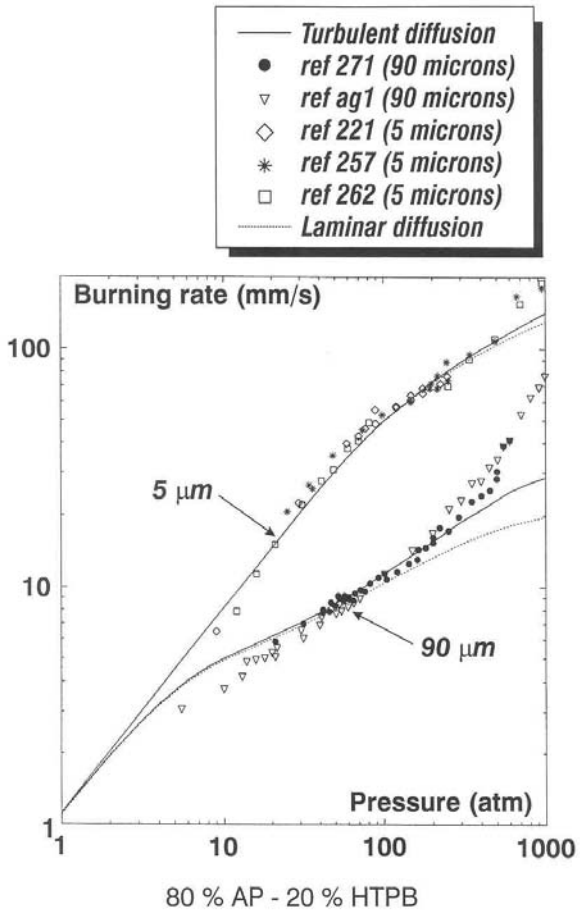


**Figure 48: Computed Burning Rates Compared to Experiments.**

For the *very small AP particle sizes* the final flame is mostly dominated by the chemical process, very sensitive to pressure, as is the AP flame. This results in a variation of the burning with a pressure exponent close to 1.

For *large particle sizes* the final flame is dominated by the diffusion process, which is insensitive to pressure. This, combined with the pressure dependent flame of the AP, see Fig. 38, gives rise to a propellant burning rate which is moderately sensitive to pressure. It is found in the modeling that the contribution of the turbulent diffusion, see Eq. (20), becomes important above about 100 atm. However above 300 to 400 atm the burning rate of the propellant undergoes a sharp exponent break that the model cannot follow. In some references this exponent break has been assumed to be due to the burning rate of the AP which would also increase sharply. It has been seen on Fig. 20 that, when the samples are carefully inhibited, this is not the case.

The strong influence of the AP particle size upon the propellant burning rate, as expressed by the modeling, is also shown on Fig. 49. It is seen that at about 1 μm there is no further gain in the burning rate. This is due to the fact that there will always exist a non vanishing flame stand-off distance related to the chemical time for the $O_2$-hydrocarbons reaction.

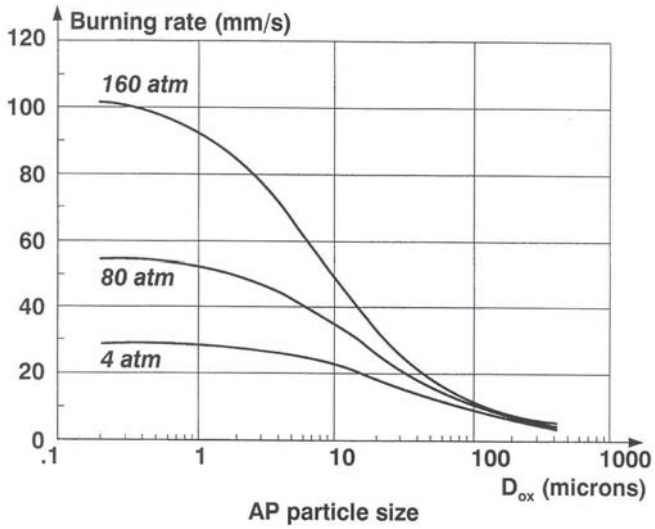


**Figure 49: Computed Burning Rate vs AP Particle Size (80 % AP – HTPB).**

On Fig. 50 the burning rate computed from the mechanisms modeled as described above is compared to results from the literature [38, 39] for mixed AP particle sizes. The agreement is adequate for the larger particle sizes and approximate for the small ones (Now, how representative are the particle sizes indicated?). This reveals that the physico-chemical features incorporated in the model of the AP-inert binder propellant are probably sound. However, once a model has been "tuned" to represent a set of experimental results, as on Fig. 48, it cannot be expected that it will "predict" very accurately other results for different values of the parameters.

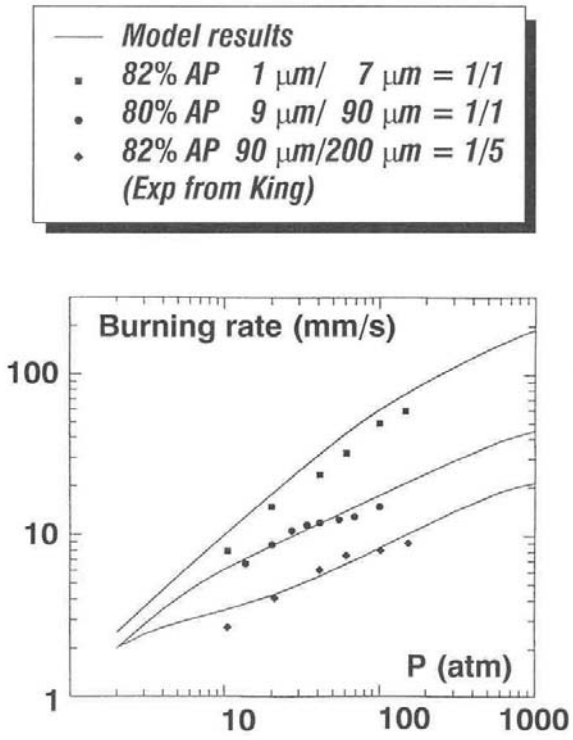


**Figure 50: Multi-Modal AP Propellants.**

It has been seen that by acting upon the AP particle size it is possible to tailor the burning rate of the propellant, but that there exist a limiting size below which the effect will be non existent, Fig. 49. It is possible to gain further by incorporating *metallic additives*, Fig. 51, such as of the ferrocenic type (which during processing will dissolve into the not yet cross-linked binder for a proper mixing). There also exist a polybutadiene binder which incorporates within its chemical structure the ferrocenic pattern (to avoid migration problems). Various results, and in particular the similarity of action of a silicon binder which produces on the propellant surface a fine structure of $SiO_2$ residue, to which it can hardly be attributed a catalytic efficiency, indicate that the mode of action of the additive is probably physical (rather than catalytic, in the sense of enhancing some chemical reactions). The layer of residue deposited on the surface has probably a flame-holding effect, the gases flowing in tortuous paths through this residue will react closer to the surface, with the final temperature not being modified, in such a way that an enhanced heat flux will act on the surface. This is taken into account in the model by decreasing the diffusion flame height, see Eq. (18), by a given factor throughout the pressure range.

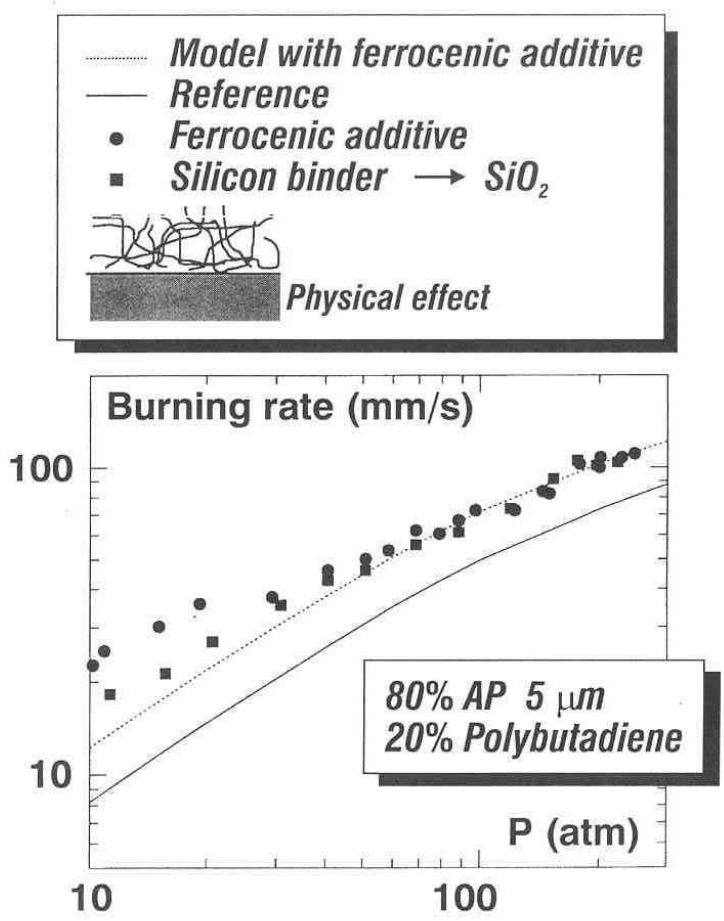


**Figure 51: Additive Modified Propellant.**

Finally, the procedure to describe the combustion of AP composite propellants is applied to a practical propellant containing two AP particle sizes and aluminum. It is observed on Fig. 52 that the presence of aluminum, which has been seen to burn far away from the surface in such a manner that no significant conductive heat flux from its flame zone goes back to the propellant surface, should be taken into account by adding a radiative heat flux as measured in Ref. [52] for propellants very close to the ones considered here. It is found then that the experimental burning rate law is followed quite well.

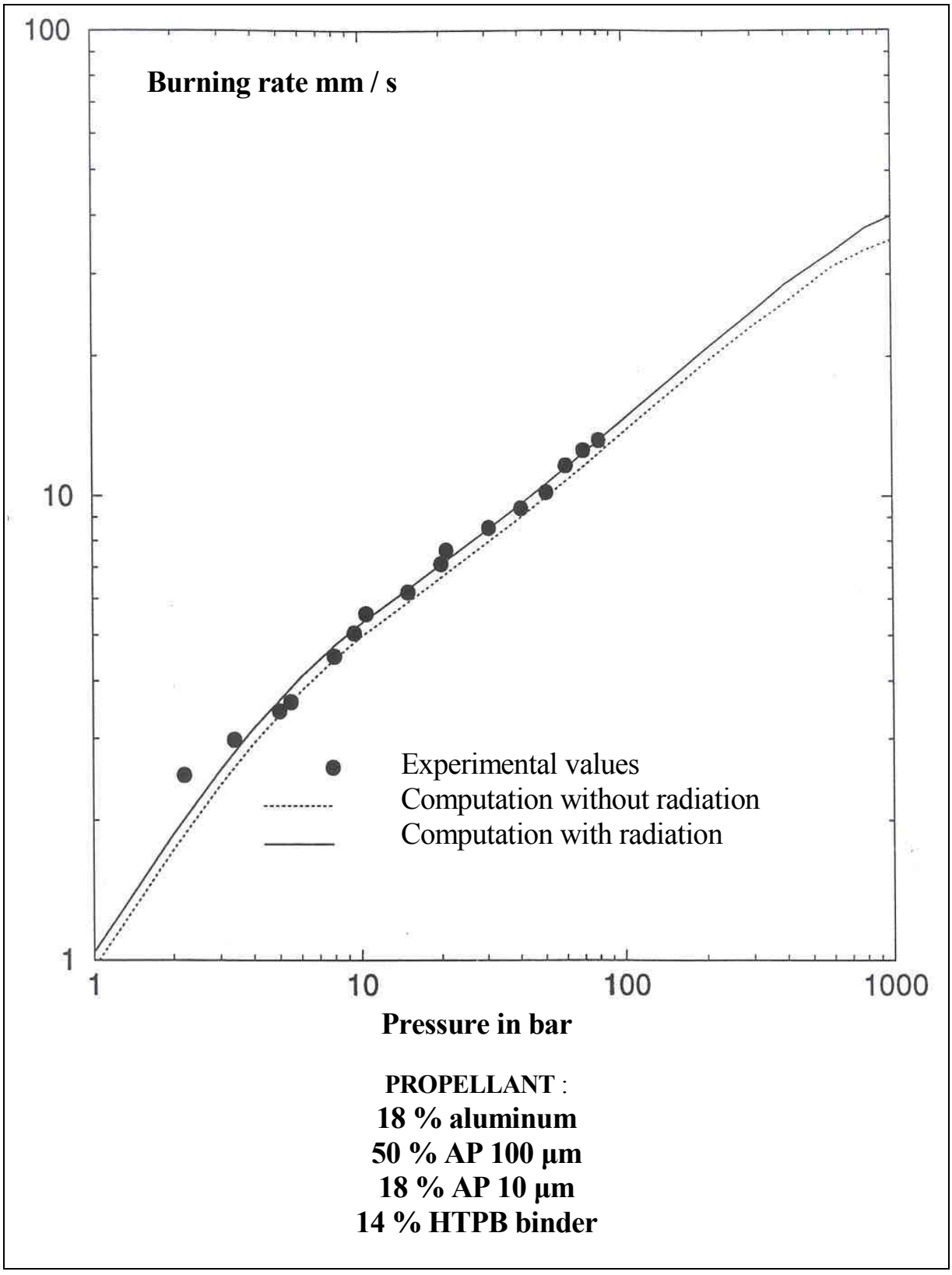


Figure 52: Burning Rate of an Industrial Propellant.

## CONCLUSIONS

A review has been presented of the viewpoint of the authors on the combustion mechanisms of components and of solid propellants. Some noteworthy points are stressed here.

*Double-Base Propellants and Active Binders:*

A fairly good knowledge of the processes in the condensed and gas phases has been acquired. The main point is the presence of a two-flame system, involving $NO_2 \rightarrow NO \rightarrow N_2$, collapsing into one flame above 200 to 300 atm. Specific additives (lead and copper salts and carbon black) have a true chemical interaction, that is the enhancement of the NO-carbon reaction, bringing some of the energy normally evolved in the second flame closer to the surface. This knowledge carries over to the active binders, which are however less prone to super-rate effects because they produce less structured carbon residue.

*Inert Binders:*

Not so many reliable pyrolysis measurements have been performed on actual binders. It has been shown (from comparisons for a number of materials) that the pyrolysis characteristics obtained at low heating rate (by thermogravimetric analysis or differential scanning calorimetry) should extrapolate and apply under combustion conditions. The mechanism of pyrolysis is a thermal breaking ( not influenced by pressure) of the cross-links and of the polymer, not affected by additives.

*Ammonium Perchlorate:*

It is believed that the mechanism of combustion is properly known. A large amount, about 70 %, of the AP exothermically decomposes in a thin (≈ 1 μm) condensed phase superficial layer, the remaining 30 % sublimes into $NH_3$ and $HClO_4$ which react in a flame very close (a few μm) to the surface. Due to the thickness, and the very short residence time associated, of these zones, additives have no true catalytic (i.e. chemical) action.

*HMX, RDX and HNIW:*

The combustion of HMX (or RDX) is qualitatively comparable to that of a DB propellant, with the occurrence of two flames, involving $NO_2$ and $N_2O/NO$. However above 20 atm these flames collapse into one and therefore it is not possible to induce super-rate effects with specific additives, as was the case for DB propellants. Also, additives which were hoped to accelerate the melting-decomposition of HMX fail to act under combustion characteristics. The burning of HNIW, the new caged nitramine, seems to be of the same nature, with a condensed phase decomposition due to thermal degradation and probably no evaporation phenomenon; also the gas flame is probably very quickly collapsed into a single overall flame, with therefore no possibility of additive effect of the double base type.

*AP or HMX Inert or Active Binder (Aluminum) Propellants:*

The approach believed to describe adequately the combustion of composite propellants is a sequential one. When following a path through the propellant, it meets successively the combustion of the oxidizer particles and of the binder layers.

In the case of *AP-inert binder propellants*, the propellant burning rate is an average of the components' rates. However an interaction flame between $O_2$ from AP and hydrocarbons from the binder enhances the rate of AP and allows the pyrolysis of the binder. The burning rate of the propellant can be quite widely tailored by reducing the AP particle size and further by adding metallic compounds which leave an oxide residue layer, the action of which is likely to be a flame holding effect, i.e. a physical action. Aluminum

incorporated in such propellants of course increases the final temperature by as much as 1000 K, but its combustion is so far from the surface that it does not influence much the regression rate of the propellant.

In the case of *HMX – RDX – or HNIW - active binder propellants*, both components have autonomous burning rates. The resulting propellant burning rate is the average of the two rates, with a further slowing down due to the fact that the HMX, or other nitramine, particles, upon reaching the surface, have to undergo a transition to full combustion. This delay is of importance up to roughly 150 atm; above it tends to become negligible. No additives have been found to act on HMX and additives of the DB type act only moderately on the active binder. The tailorability of HMX, or other nitramine, - active binder propellants is therefore more limited than for AP propellants.

*Further trends on new ingredients* are related in the first place to the need to reduce the vulnerability to various aggressions of missile motors employing solid propellants: "cook off" due to fires, bullet or fragment impact, "sympathetic detonation". Another emerging concern is that of the pollution caused by the large boosters of space launchers, using AP - inert binder - aluminum propellants, with production of HCl and $Al_2O_3$ smoke.

These considerations have led to reconsidering ingredients such as ammonium nitrate, $NH_4NO_3$, discarded previously as being insufficiently energetic, reconsidered and seemingly not considered any longer, and to introducing energetic binders such as GAP, glycidyl azide polymer (containing the $N_3$ group, inducing an exothermic decomposition), briefly mentioned in the text, or oxidizers containing the $N\text{-}NO_2$ group while being less sensitive than HMX or RDX, such as ADN ($NH_4\text{-}N\text{-}(NO_2)_2$).

Also considered are caged nitramines, such as CL20 (also called HNIW), which maintains the energetic level with a lesser amount of oxidizer, thus reducing the vulnerability, or which allows a higher energetic level. A number of new results on this component has been presented in the text.

It is hoped that the large amount of information gathered and the understanding acquired about the already used propellants ingredients will allow an efficient approach to the mastering of the behavior of the new ingredients and the corresponding propellants.

## ACKNOWLEDGEMENTS

The work of ONERA has been carried out in large part under contracts from the Délégation Générale à l'Armement (M.S. Amiet) and in cooperation with the Société Nationale des Poudres et Explosifs (R. Couturier, Y. Longevialle and colleagues) and with the Ecole Nationale Supérieure des Techniques Avancées (E. Cohen-Nir).

J.C. Amiot and J. Hommel have actively participated in the experimental work.

The authors acknowledge the efforts of Y. Le Breton and F. Laroche in elaborating the manuscript.

Much information was exchanged, in particular through the then AGARD consultant program, with M.W. Beckstead, Brigham Young University, M.Q. Brewster, University of Illinois – Urbana Champaign, and N.S. Cohen, consultant.

## REFERENCES

This document is very much extracted from:

- G. Lengellé: "Recent Developments and Challenges in Ignition and Combustion of Solid Propellants". Invited plenary conference, 4th International Symposium in Chemical Propulsion,

Stockholm, May 1996. Publication in 1997 "Challenges in Propellants and Combustion", Begell House, New York.

- G. Lengellé, J. Duterque and J.F. Trubert: "Physico-Chemical Mechanisms of Solid Propellant Combustion". Contribution to "Solid Propellant Chemistry, Combustion and Motor Interior Ballistics", Volume 185, Progress in Astronautics and Aeronautics, AIAA, 2000.

## General References (Combustion, Chemical Propulsion, Solid Propellants)

- Williams F.A., *Combustion Theory* (Second Edition), Benjamin/Cummings Publishing Co, Menlo Park, 1985.
- Kuo K.K., *Principles of Combustion*, John Wiley and Sons, New York, 1986.
- Williams F.A., Barrère M. and Huang N.C., *Fundamental Aspects of Solid Propellant Rockets*, AGARD 116, 1969.
- Timnat Y.M., *Advanced Chemical Rocket Propulsion*, Academic Press, London, 1987.
- Kuo K.K. and Summerfield M. (Eds), *Fundamentals of Solid Propellant Combustion*, Volume 90 of Progress in Astronautics and Aeronautics, 1984.
- Yang V. and Zarko V.E. (Eds), "Solid Propellant Motor Interior Ballistics and Combustion of Energetic Materials", Special issue of Journal of Propulsion and Power, Vol. 11, n° 4, July-August 1995.
- Yang V., Brill T.B. and Ren W.Z., *Solid Propellant Chemistry, Combustion and Motor Interior Ballistic*, Volume 185 of Progress in Astronautics and Aeronautics, 2000.

## Double-Base Propellants and Active Binders References

[1] Heller C.A. and Gordon A.S., "Structure of the Gas Phase Combustion Region of a Solid Double-Base Propellant", The Journal of Physical Chemistry, Vol. 59, n° 8, pp. 773-777, 1955.

[2] Zenin A.A., "Structure of Temperature Distribution in Steady-State Burning of a Ballistite Powder", Combustion, Explosion and Shock Waves, Vol. 2, n° 3, pp. 67-76, 1966.

[3] Kubota N., Ohlemiller J.J., Caveny L.H. and Summerfield M., "The Mechanism of Super-Rate Burning of Catalyzed Double-Base Propellants", 15th Symposium (International) on Combustion, pp. 529-537, The Combustion Institute, 1975.

[4] Kubota N. and Ishihara A., "Analysis of the Temperature Sensitivity of Double-Base Propellants", 20th Symposium (International) on Combustion, pp. 2035-2041, The Combustion Institute, 1984.

[5] Lengellé G., Bizot A., Duterque J. and Trubert J.F., "Steady-State Burning of Homogeneous Propellants", in Fundamentals of Solid-Propellant Combustion (Ed. K.K. Kuo and M. Summerfield), Vol. 90 of Progress in Astronautics and Aeronautics, 1984.

[6] Duterque J., Hommel J. and Lengellé G., "Experimental Study of Double-Base Propellants Combustion Mechanisms", Propellants, Explosives, Pyrotechnics, Vol. 10, pp. 18-25, 1985.

[7] Trubert J.F., "Analysis of the Condensed Phase Degradation Gases of Energetic Binders", La Recherche Aérospatiale, 1989, n° 2 (March-April), pp. 69-79; AGARD/PEP Specialists Meeting on Smokeless Propellants, Florence, September 1985, AGARD C.P. n° 391.

[8] Lengellé G., "Thermal Degradation Kinetics and Surface Pyrolysis of Polymers", AIAA Journal, Vol. 8, n° 11, pp. 1989-1996, 1970.

[9] Bizot A. and Beckstead M.W., "A Model for Double-Base Propellant Combustion", 22nd Symposium (International) on Combustion, pp. 1827-1834, The Combustion Institute, 1988.

[10] Cohen N.S. and Lo G.A., "Combustion Chemistry of Nitrate Ester-Based Propellants", AIAA Paper 83-1198, June 1983; 20th JANNAF Combustion Meeting, October 1983.

[11] Song Y.H., Beer J.M. and Sarofim A.F. "Reduction of Nitric Oxide by Coal Char at Temperatures of 1250-1750 K", Combustion Science and Technology, Vol. 25, pp. 237-240, 1981.

[12] Youfang C., "Combustion Mechanism of Double-Base Propellants with Lead Burning Rate Catalysts", Propellants, Explosives, Pyrotechnics, Vol. 12, pp. 209-214, 1987.

## Inert Binders References

[13] Madorsky S.L., *Thermal Degradation of Organic Polymers*, Interscience Publishers, New York, 1964.

[14] Jellinek H.H.G., *Aspect of Degradation and Stabilization of Polymers*, Elsevier Scientific Publishing Co, New York, 1978.

[15] Strand L.D., Jones M.D. and Ray R.L., "Characterization of the Hybrid Rocket Internal Flux and HTPB Fuel Pyrolysis". AIAA Paper 94-2876, 30th Joint Propulsion Conference, Indianapolis, June 1994.

[16] Cohen N.S., Fleming R.W. and Derr R.L., "Role of Binders in Solid Propellant Combustion", AIAA Journal, Vol. 12, n° 2, pp. 212-218, 1974.

[17] Beck W.H., "Pyrolysis Studies of Polymeric Materials Used as Binders in Composite Propellants: A Review", Combustion and Flame, Vol. 70, pp. 171-190, 1987.

## Ammonium Perchlorate References

[18] Levy J.B. and Friedman R., "Further Studies of Pure Ammonium Perchlorate Deflagration", 8th Symposium (International) on Combustion, pp. 663-672, The Combuston Institute, 1962.

[19] Guirao C. and Williams F.A., "A Model for Ammonium Perchlorate Deflagration between 20 and 100 atm", AIAA Journal, Vol. 9, n° 7, pp. 1345-1356, 1971.

[20] Beckstead M.W., Derr R.L. and Price C.F., "The Combustion of Solid Monopropellants and Composite Propellants", 13th Symposium (International) on Combustion, pp. 1047-1056, The Combustion Institute, 1971.

[21] Price C.F., Boggs T.L. and Derr R.L., "The Steady State Combustion Behavior of Ammonium Perchlorate and HMX", AIAA paper n° 79-0164, 17th Aerospace Sciences Meeting, 1979.

[22] Godon J.C., "Model of Ammonium Perchlorate Self-Deflagration", La Recherche Aérospatiale, 1982-2, pp. 43-50.

[23] Seleznev V.A., "An Optical Method of Measuring the Burning Surface Temperature of Condensed Systems", Combustion and Flame, Vol. 13, n° 2, 1969.

## HMX, RDX, HNIW References

[24] Rogers R.N., "DSC Determination of the Kinetics Constants of Systems that Melt with Decomposition", Thermochemica Acta, Vol. 3, pp. 437-447, 1972.

[25] Boggs T.L., "The Thermal Behavior of RDX and HMX", in Fundamentals of Solid-Propellant Combustion (Ed. K.K. Kuo and M. Summerfield), Vol. 90 of Progress in Astronautics and Aeronautics, 1984.

[26] Cohen N.S., Lo G.A. and Crowley J.C., "Model and Chemistry of HMX Combustion", AIAA Journal, Vol. 23, n° 2, p. 276, 1985.

[27] Kubota N. and Sakamoto S., "Combustion Mechanism of HMX", 19th International Annual Conference of ICT, Karlsruhe, June 1988.

[28] Mitani T. and Williams F.A., "A Model for the Deflagration of Nitramines", 21st Symposium (International) on Combustion, pp. 1965-1974, The Combustion Institute, 1986. Also, Sandia Report 86-8230, December 1986.

[29] Lengellé G. and Duterque J., "Combustion of Propellants Based on HMX", AGARD/PEP Specialists' Meeting on Smokeless Propellants, AGARD CP n° 391, Florence, September 1985.

[30] Bizot A. and Beckstead M.W., "A Model for HMX Combustion", International Seminar on Flame Structure, Alma-Ata (Former USSR), September 1989.

[31] Shoemaker R.L. et al, "Thermophysical Properties of Propellants", Thermal Conductivity, Vol. 18, pp. 199-211, 1985.

[32] Hatch R.L., "Chemical Kinetics of HMX Combustion", 24th JANNAF Combustion Meeting, Monterey, Cal., October 1987.

[33] Brill T.B., "Heat Flow / Chemistry Interface in the Condensed phase (HMX)", ONR Workshop on Energetic Material Initiation Fundamentals, Livermore, Cal., December 1988.

[34] Liau Y.C. and Yang V., "Analysis of RDX Monopropellant Combustion with Two-Phase Subsurface Reactions", Journal of Propulsion and Power, Vol. 11, July 1995, p. 729.

[35] Longevialle Y., Golfier M. and Graindorge H., "New Generation of Propellants for High Performances Solid Rocket Motors", RTO / AVT Symposium Small Rocket Motors, 1999.

[36] Trubert J.F. and Hommel J., "Study of the Condensed Phase Degradation and Combustion of Two New Energetic Charges for Low Polluting and Smokeless Propellants: HNIW and ADN", ICT Annual Conference, June 2002.

## Composite Propellants References

[37] Beckstead M.W., Derr R.L. and Price C.F., "A Model of Composite Solid-Propellant Combustion Based on Multiple Flames", AIAA Journal, Vol. 8, n° 12, pp. 2200-2207, 1970.

[38] Cohen N.S., "Review of Composite Propellant Burn Rate Modeling", AIAA Journal, Vol. 18, n° 3, pp. 277-293, 1980.

[39] Cohen N.S. and Strand L.D., "An Improved Model for the Combustion of AP Composite Propellants", AIAA paper n° 81-1553, 17th Propulsion Conference, 1981.

[40] Ramohalli K.N.R., "Steady State Burning of Composite Propellants", in Fundamentals of Solid-Propellant Combustion (Ed. K.K. KUO and M. Summerfield), Vol. 90 of Progress in Astronautics and Aeronautics, 1984.

[41] Cohen N.S., Crowley J.C. and Lo G.A., "Effects of HMX Addition on the Combustion of Energetic Binders", 21st JANNAF Combustion Meeting, October 1984.

[42] Beckstead M.W. and McCarty K.P., "Modeling Calculations for HMX Composite Propellants", AIAA Journal, Vol. 20, n° 1, pp. 106-115, 1982.

[43] Duterque J. and Lengellé G., "Combustion Mechanisms of Nitramine Based Propellants with Additives", AIAA paper n° 88-3253, 24th Propulsion Conference, 1988. Journal of Propulsion and Power, Vol. 6, n° 6, pp. 718-726, December 1990.

[44] Blomshield F. and Osborn J., "Nitramine Composite Solid Propellant Modeling", AIAA paper n° 90-2311, 26th Propulsion Conference, 1990.

[45] Beckstead M.W., "A Model for Composite Modified Double-Base Propellant Combustion", 26th JANNAF Combustion Meeting, October 1989.

[46] Cohen N.S., "A Pocket Model for Aluminum Agglomeration in Composite Propellants", AIAA Journal, Vol. 21, n° 5, pp. 720-725, 1983.

[47] Price E.W., "Combustion of Metalized Propellants", in Fundamentals of Solid-Propellants Combustion (Ed. K.K. Kuo and M. Summerfield), Vol. 90 of Progress in Astronautics and Aeronautics, 1984.

[48] Duterque J., "Experimental Studies of Aluminium Agglomeration in Solid Rocket Motors", 4th International Symposium on Special Topics in Chemical Propulsion, Stockholm (Sweden), 1996, Begell House Inc. Publisher.

[49] Renie J.P. and Osborn J.R., "Combustion Modeling of Aluminized Propellants", AIAA paper n° 79-1131, 15th Propulsion Conference, 1979.

[50] Lengellé G., Fourest B., Godon J.C. and Guin C., "Condensed Phase Behavior and Ablation Rate of Fuels for Hybrid Propulsion", AIAA paper n° 93-2413, 29th Propulsion Conference, 1993.

[51] Trubert J.F., Duterque J. and Lengellé G., "Study of the Condensed Phase Degradation and Combustion of Glycidyl Azide Polymer", ICT Annual Conference, June 1999.

[52] Ishihara A., Brewster M.Q., Sheridan T.A. and Krier H., "The Influence of Radiative Heat Feedback on Burning Rate in Aluminized Propellants", Combustion and Flame Vol. 84, pp. 141-153, 1991.